Measurements of the extension required for crustal breakup on the magma-poor Iberia-Newfoundland conjugate margins

Júlia Gómez-Romeu[1,*], Nick Kusznir[1,2], Alan Roberts[2] & Gianreto Manatschal[3]

[1]*Department of Earth, Ocean and Ecological Sciences, University of Liverpool, Liverpool, UK*

[2]*Badley Geoscience Ltd, Spilsby, UK*

[3]*Institut de Physique du Globe de Strasbourg-EOST, Université de Strasbourg-CNRS, France*

[*]*Currently:* M&U sas, *Saint-Égrève, France*

Abstract

Rifted margins have been extensively studied, however there are still many important questions related to their formation processes. We use the Iberia-Newfoundland conjugate rifted margins as a natural laboratory to investigate how much extension is required to produce crustal rupture and separation. To achieve our aim we use; (i) gravity anomaly inversion to measure continental crustal thinning, (ii) subsidence analysis to measure continental lithosphere thinning and (iii) fault heave summation from seismic observations to obtain brittle continental crust extension. Integration of thinning from gravity anomaly inversion and subsidence analysis is used to determine continental crust extension and continental lithosphere extension respectively. These measurements have been made between the proximal continental crust and the distal Limit of Contiguous Continental Crust (LCCC) on the northern (SCREECH1 and ISE01) and the southern (SCREECH2 and TGS/LG12) conjugate seismic profiles. For the Iberia-Newfoundland conjugate rifted margins, extension values determined from the integration of crustal and lithosphere thinning are similar and suggest that on average 172 km of extension is required to produce crustal breakup. In contrast, measured extension from fault heave summation is on average 128 km which indicates an apparent extension discrepancy at the scale of the whole conjugate margin system when observed brittle continental crust extension is compared with lithosphere and crust extension.

Fault population analysis shows that sub-seismic resolution faulting significantly contributes to an under-estimate of brittle crustal extension by up to 25%. Allowing for fault extension at sub-seismic resolution indicates that an extension discrepancy at the scale of the whole conjugate margin system does not exist. Fault geometries and the location of the distalmost contiguous continental crust are also important issues that should be carefully considered when comparing fault heave summation and extension from crust and lithosphere thinning.

The absence of an extension discrepancy between fault extension, crustal extension and lithosphere extension at the scale of a whole conjugate margin system should not be confused with the presence of depth-dependent stretching and thinning at a given location on the margin which is both expected and observed at rifted continental margins.

1. Introduction

How much extension is required to produce crustal breakup is still poorly understood. Crustal breakup occurs due to progressive continental lithosphere stretching and thinning achieved by two main processes, brittle faulting deformation within the upper crust with underlying more distributed deformation within the lower crust and upper mantle. A range of methodologies can be used to measure extension at rifted continental margins appropriate to different depths within the lithosphere (see Figure 4.1 in Davis and Kusznir, 2004). These methods include section balancing, extension derived from crustal thinning and lithosphere thinning, and fault heave summation. Fault heave summation has been applied to the Iberia margin by Davis and Kusznir (2004) and Reston (2005) while Reston and McDermott (2014) and Lymer et al., (2019) have carried out the same process at different lateral length scales. Others such as Ranero and Pérez-Gussinyé (2010) applied section balancing to the Iberia margin.

To date the only studies that have determined the total extension for crustal breakup for conjugate margin pairs are those of Sutra et al., (2013) who used section balancing and Jeanniot et al., (2016) who used forward kinematic modelling calibrated by observed water loaded bathymetry and crustal thickness profiles. Both of these studies were applied to the same Iberia-Newfoundland conjugate margin profiles but reported different total extension values for breakup. For the SCREECH1 - ISE01 conjugate margin profile Sutra et al., (2013) gave 256 km while Jeanniot et al., (2016) gave 175 km. For the SCREECH2 – TGS/LG12 profile their reported values were 229 km and 160 km respectively.

In this study we apply three independent methods to analyse the SCREECH1 - ISE01 and SCREECH2 – TGS/LG12 profiles and measure the amount of extension to achieve crustal breakup and separation for the Iberia-Newfoundland rift system.

Extensional faults at rifted margins have been studied by direct observations using seismic data and field observations. In contrast the deeper distributed pure-shear deformation is not directly observed and consequently numerical models are required to simulate it. On this basis, it has been often assumed that extensional faults are the most important means by which continental lithosphere extends simply because they are visible. In order to conserve mass, the stretching of the upper continental crust by extensional faulting is assumed to be the same as the whole continental crust and lithosphere; i.e. extensional faulting and deeper distributed pure-shear deformation must balance at the scale of the whole conjugate margins. In contradiction with this assumption, depth-dependent stretching and thinning, in which the upper lithosphere is less extended than that of the whole lithosphere, has been observed within the proximal and necking domains of rifted margins (e.g. Driscoll and Karner 1998; Roberts et al., 1997; Baxter et al., 1999; Davis and Kusznir, 2004; Kusznir and Karner, 2007). An important question is whether the amount by which continental crust is extended by brittle faulting is less than that of the whole continental crust and lithosphere at the scale of a whole conjugate pair of rifted margins.We investigate whether the observed brittle fault extension from seismic reflection observations differs or equals the measured whole-lithosphere and whole-crust extension at the scale of a conjugate rifted margins system. To achieve our aim, we use the Iberia-Newfoundland conjugate rifted margins and apply a gravity anomaly inversion method to quantify continental crustal thinning and a subsidence analysis technique to measure continental lithosphere thinning. Integration of thinning from gravity anomaly inversion and subsidence analysis is used to determine continental crust extension and continental lithosphere extension respectively. We use seismic interpretation to measure brittle extension from fault heave summation. These measurements have been made between the proximal and distalmost contiguous continental crust for the conjugate margins. We also investigate the importance of sub-seismic resolution fault extension when comparing fault heave summation with lithosphere and crust extension.

2. The Iberia-Newfoundland conjugate rifted margins

The conjugate Iberia-Newfoundland rifted margins are an ideal natural laboratory because they are both sediment and magma starved and are among the best studied rifted margin

systems worldwide. The Iberia-Newfoundland margins have undergone a polyphase evolution characterized by an earlier rift event during Late Triassic to Early Jurassic followed by a later rift event during Middle-Late Jurassic to Early Cretaceous. The age of continental lithosphere breakup for these margins has been suggested to be between 112 Ma (Péron-Pinvidic et al., 2007), 115 Ma (Eddy et al., 2017) and 126 Ma (Russell and Whitmarsh, 2003; Manatschal, 2004). We focus on two pairs of conjugate seismic profiles along these margins; one across the Galicia Bank-Flemish Cap (i.e. northern profiles consisting of SCREECH1 – ISE01 seismic lines, Funck et al., 2003; Zelt et al., 2003, Figure 1a) and the other one across the southern Iberia Abyssal Plain-Flemish Pass (i.e. southern profiles consisting of SCREECH2 – TGS/LG12 seismic lines, Beslier, 1996; Shillington et al., 2006; Sutra et al., 2013, Figure 1b).

3. Measuring thinning and extension of continental crust and lithosphere

We use quantitative techniques consisting of gravity anomaly inversion and subsidence analysis to measure continental crustal thinning and continental lithosphere thinning respectively. Integration of thinning from gravity anomaly inversion and subsidence analysis is used to determine total continental crust extension and total continental lithosphere extension respectively from proximal margin to the distal limit of contiguous continental crust. We apply both techniques to the northern and southern seismic profiles of the Iberia-Newfoundland conjugate rifted margins.

3.1. Gravity anomaly inversion: thinning and extension of continental crust

Gravity anomaly inversion has been used to determine the depth to the Moho, crustal thickness and continental crustal thinning using a method that incorporates a correction for the lithosphere thermal gravity anomaly. The method and its applications is described in detail elsewhere (Chappell and Kusznir, 2008; Alvey et al., 2008; Kusznir et al., 2018). Input data used for the gravity anomaly inversion are: (i) satellite free-air gravity anomaly data (Sandwell and Smith 2009 and subsequent updates at http://topex.ucsd.edu/www_html/mar_grav.html), (ii) bathymetric/topographic data (Smith and Sandwell 1997 and subsequent updates at http://topex.ucsd.edu/www_html/mar_topo.html), (iii) regional sediment thickness data (Divins 2003 and subsequent updates at http://www.ngdc.noaa.gov/mgg/sedthick/sedthick.html) and locally 2D sediment thickness

obtained from both the northern (SCREECH1 – ISE01) and southern (SCREECH2 – TGS/LG12) seismic profiles of the Iberia and Newfoundland conjugate rifted margins and (iv) age of ocean isochrons from Müller et al., (2008).Gravity anomaly inversion has been carried out in the 3D spectral domain to determine Moho topography from free-air gravity corrected for bathymetric and sedimentary contributions (assuming compaction-controlled sediment density) using the scheme of Parker (1972). A Butterworth filter with a 100 km wavelength cut-off is applied prior to the inversion for Moho depth. For the long wavelength gravity anomaly components to be included in the 3D gravity inversion arising from the lithosphere thermal anomaly and relief in, bathymetric, top basement and Moho relief, a large map area is used. For the Iberia margin this is between 8^{o}W to 15^{o}W and 36^{o} N to 45^{o}N, and for the Newfoundland margin between 40^{o}W to 49^{o}W and 42^{o} N to 52^{o}N.

By invoking Smith's theorem (Smith, 1961), for the assumptions made, this provides a unique solution for the 3D Moho topography (see Chappell and Kusznir, 2008 for more detailed explanation). We use constant crustal density of 2850 kg/m^{-3} (averaged from Carlson and Herrick, 1990; Christensen and Mooney, 1995) and a mantle density of 3300 kg/m^{-3} (Jordan and Anderson, 1974). To determine Moho depth from gravity inversion, a reference Moho depth is needed and requires calibration against seismic refraction Moho depths (see Cowie et al., 2015 for a detailed discussion). We use a reference Moho depth of 40 km for the Iberia margin (Cowie et al., 2015) while 37.5 km is used for the Newfoundland margin (Jeanniot et al., 2016). An initial thickness of continental crust of 37.5 km is used for both the Iberia and Newfoundland margins.

Key to the gravity anomaly inversion method is a correction for the lithosphere thermal gravity anomaly (Chappell and Kusznir, 2008) associated with the elevated lithosphere geotherm resulting from rifting/breakup of the margin. Failure to include this correction leads to a substantial overestimate of Moho depth and crustal basement thickness and an underestimate of continental crustal thinning. The lithosphere thermal gravity anomaly is obtained from the present-day 3D lithosphere thermal anomaly. This is calculated from the initial lithosphere thermal perturbation and the thermal re-equilibration time. The initial thermal perturbation is calculated from the lithosphere thinning factor (γ=1-1/β) derived iteratively from crustal thinning determined by gravity inversion assuming depth uniform stretching and thinning. For ocean lithosphere, the lithosphere thermal equilibration time corresponds to the age of the oceanic lithosphere obtained from ocean isochrons (Müller et al., 2008) while for continental margin lithosphere the breakup age is taken. Ocean isochrons

are only used to give the thermal re-equilibration time of oceanic lithosphere, they are not used to define the COB for which they are unreliable. In this study, a lithospheric breakup age of 120 Ma is used, consistent with Cowie et al., (2015). Tests using breakup ages of 115 and 125 Ma show only small sensitivity to breakup age because the rifted margin and adjacent oceanic lithosphere is almost thermally re-equilibrated.

During rifting and breakup decompression melting leads to magmatic addition which thickens the thinned continental crust and eventually forms oceanic crust. The thickness of the magmatic addition is determined using a parameterization of the decompression melting model of White and McKenzie (1989) together with the continental lithosphere thinning factor (γ=1-1/β) obtained from the gravity anomaly inversion (see Chappell and Kusznir, 2008 for further details). In this study we use a parameterization of "normal" decompression melting in which melting commences at γ = 0.7 and produces 7 km of melt at γ = 1 corresponding to the average thickness of oceanic crust (Grevemeyer et al., 2018). We also use an alternative parameterization which represents the effect of serpentinization of mantle exhumed at a magma starved margin which produces a mass deficiency equivalent to 3.1 km of crustal basement (see Cowie et al. 2015 for further details). Figure 2 summarizes the results obtained from the gravity anomaly inversion applied along the northern (Figure 2a) and the southern (Figure 2e) profiles. Figures 2b and 2f show the present-day crustal architecture of the Iberia and Newfoundland margins consisting of seabed and top basement interpreted on the seismic data and Moho depth obtained from the gravity anomaly inversion using a "normal" magmatic parameterization for decompression melting. The crustal thinning factor from gravity anomaly inversion using "normal" and serpentinized mantle parameterizations is shown in Figures 2c and 2g.

Along the four profiles analysed in this study there are seismic measurements of Moho depth that can be compared with Moho depths determined by our gravity inversions. Refraction seismic velocity models produced by Funck et al., (2003) along profile SCREECH1 show similar Moho depths to that from our gravity inversion for the proximal margin where Moho depths are 30-32 km and 31-33 km respectively. In the distal COB region refraction seismology gives a depth to the 8.0 km/s^{-1} iso-velocity contour of 12.5 km, corresponding to top mantle, compared with 11-12 km from gravity inversion. The refraction seismic velocity model obtained by Van Avendonk et al., (2006) along profile SCREECH2 shows Moho depth in the proximal region just less than 30 km while gravity inversion gives 30 km at the same place. In the distal COB region, seismic refraction gives a depth to iso-velocity 8.0

189 km/s^{-1}, corresponding to top mantle, of 12 km while gravity inversion gives a Moho depth of
190 between 11 and 13 km. For the Newfoundland margin the Moho depths from gravity
191 inversion and refraction seismology are consistent.

192 On the Iberian margin, adjacent to our southern profile (TGS/LG12), the seismic refraction
193 results of Chian et al., (1999) give a Moho depth of 12 – 13 km, which compares well with
194 the gravity Moho depth of 11 – 12 km from this study. However, this comparison lies within
195 the region of exhumed mantle and continental allochthons outboard of the most distal
196 contiguous continental crust. Similarly, the seismic studies of Davy et al., (2016) and Lymer
197 et al., (2019), which report a Moho depth of 9 km, are outboard of the contiguous continental
198 crust and our northern Iberian profile along ISE01, so a comparison cannot be made.

199 Zelt et al., (2003) carried out wide-angle seismology (FAST and wide-angle reflection) on the
200 ISE01 profile. Their reported Moho depth is substantially shallower than that determined by
201 gravity inversion. Zelt et al., (2003) show P-wave iso-velocity contours between 7 and 7.6
202 km/s^{-1}, but are not able to resolve the expected higher seismic velocities consistent with rays
203 sampling the mantle. Cowie et al., (2015) found a similar mismatch of Moho depth
204 determined from gravity inversion and that reported by Zelt et al., (2003) and discussed in
205 detail the causes that may produce the mismatch between the gravity and seismic Moho
206 depth. In places the seismic Moho depth interpreted by Zelt et al., (2003) corresponds to V_p
207 seismic velocities as low as 7.2 km/s^{-1} and Cowie et al., (2015) suggest that this may
208 correspond to the top of lower crustal igneous bodies rather than the top of the mantle. In
209 addition, the upper crustal velocity structure reported by Zelt et al., (2003) suggests that there
210 may be several km of pre-rift sediments under the base syn-rift used in this study to give the
211 sediment thickness, particularly within the Galicia Interior Basin. For the purpose of this
212 study we prefer to use sediment thickness to base syn-rift to determine crustal thinning
213 associated with Cretaceous breakup.

214 We horizontally integrate the gravity crustal thinning factor from the proximal edge of
215 continental crust until the distal end of the profile to determine crustal extension along the
216 Iberia and Newfoundland rifted margins. Crustal extension estimates resulting from the
217 integration of crustal thinning factors obtained using “normal” and serpentinized mantle
218 solutions are shown in Figures 2d and 2h. Note that crustal extension results are not
219 significantly dependent on the parameterization used to predict magmatic addition and
220 serpentinized mantle. The determined crustal extension required to generate crustal breakup

and separation is dependent on the where the integration starts at the proximal end of the profiles. For the two Iberia profiles some extension is missed because the profiles do not continue eastwards sufficiently far. We believe that this problem is relatively minor and is discussed later.

3.2. Subsidence analysis: thinning and extension of continental lithosphere

We use a subsidence analysis technique (for details see Roberts et al., 2013; Cowie et al., 2015) to obtain lithosphere thinning factors, which we compare against the crustal thinning factors from gravity anomaly inversion. This technique involves converting water loaded subsidence into lithosphere thinning factor assuming a modified McKenzie (1978) model which incorporates magmatic addition. Flexural backstripping (Kusznir et al., 1995; Roberts et al., 1998) and decompaction assuming shaly-sand parameters (Sclater and Christie, 1980) is used to remove sedimentary layers and loading to the top of pre-rift sequence and top of oceanic crust. We use a value of effective elastic thickness (Te) = 3 km in the flexural backstripping following Roberts et al., (1997). Sensitivity tests show that subsidence analysis results are not significantly sensitive to Te because the sediment load is dominated by the long wavelength post-breakup component. Flexural backstripping gives a sediment-corrected bathymetry which we equate to water-loaded subsidence assuming that top of pre-rift sequence was at sea-level prior rifting.

Backstripped water-loaded subsidence is considered to represent the sum of initial and thermal subsidence in the context of McKenzie (1978). We convert water-loaded subsidence into lithosphere thinning factor using the McKenzie (1978) model which is modified to include a correction for the isostatic effects of magmatic addition from decompression melting or serpentinized mantle. As lithosphere thinning increases syn- and post-rift subsidence increase, however at large thinning factors magmatic addition is produced by decompression melting which thickens the crust reducing the syn-rift subsidence component. Melt thickness is predicted as a function of lithosphere thinning factor using the same parameterisation of the decompression melt model of White and McKenzie (1989) used for the gravity inversion (see Roberts et al., 2013 for more details). In the case of magma-starved breakup, mantle exhumation and serpentinization occurs also reducing the syn-rift subsidence because serpentinization reduces mantle density. Serpentinized mantle has a mass deficiency equivalent to that of crust of thickness 3.1 km (see Cowie et al., 2015 for a more detailed explanation). Note that in the subsidence analysis method, as in the gravity inversion method,

lithosphere thinning and crustal thinning are assumed to be the same (i.e. depth-uniform stretching and thinning is assumed).

An initial crustal thickness of 37.5 km with crustal and mantle densities of 2850 kg/m^3 and 3300 kg/m^3 respectively are used in the subsidence analysis. A lithospheric breakup age of 120 Ma is used for the Iberia and Newfoundland margins. Sensitivity tests using breakup ages of 115 and 125 Ma do not significantly change the subsidence analysis results.

Before subsidence analysis can be carried out, a correction needs to be made to water loaded subsidence for present-day mantle dynamic topography generated by convective circulation within the deep mantle. Mismatches of top basement depth between the restored rifted margins of Iberia and Newfoundland that cannot be explained by differences in sediment loading have been reported and discussed (Funck et al., 2003; Crosby et al., 2008). They proposed that the Newfoundland margin is presently subject to mantle dynamic uplift while the Iberian margin has dynamic subsidence, although magnitudes were uncertain. The recent compilation of residual topography by Steinberger et al., (2017) indicates approximately 500 m of dynamic uplift on the Newfoundland margin where it is crossed by the SCREECH1 and SCREECH2 profiles. As a consequence we apply a correction to water loaded subsidence for present-day dynamic topography of -500 m on the Newfoundland margin. For the Iberian margin, Steinberger et al., (2017)'s residual topography on the contiguous continental crust of the LG12 and ISE01 profiles shows a zero to slightly positive (< +250 m) dynamic uplift while the distal ends show dynamic subsidence approaching -250 m. For the Iberia margin we apply a zero correction to water loaded subsidence for present-day dynamic topography.

Figure 3 summarizes the results obtained from the subsidence analysis applied along the northern and southern profiles of Iberia and Newfoundland conjugate margins. The sediment corrected bathymetry (i.e. water loaded subsidence) obtained from flexural backstripping, present-day top basement and seabed are shown in Figures 3a and 3d. The lithosphere thinning factors determined from subsidence analysis using "normal" and serpentinized mantle parameterizations are shown in Figures 3b and 3e.

In order to determine lithosphere extension, we horizontally integrate the continental lithosphere thinning factor derived from subsidence analysis from the proximal continental start to distal end of the profiles across the Iberia and Newfoundland rifted margins. Lithosphere extension estimates resulting from the integration of lithosphere thinning factors obtained using "normal" and serpentinized mantle solutions are shown in Figures 3c and 3f.

Note that lithosphere extension results are not significantly dependent of the parameterization used to predict magmatic addition and serpentinized mantle. As with the integration of crustal thinning factor derived from gravity inversion, extension is dependent on the proximal starting point of the integration which is limited by the extent of the seismic profiles. The implication of missing extension from proximal thinning factor integration is discussed later.

4. Continental lithosphere and crustal extension required for crustal breakup

The process of continental breakup leading to the formation of a rifted margin has been discussed by many authors (e.g. Cannat et al., 2009; Huismans and Beaumont, 2011; Brune et al., 2012; Soares et al., 2012; Sutra et al., 2013; Haupert et al., 2016; Gillard et al., 2017; Alves and Cunha, 2018). Continental breakup has many different definitions; when continental crust is ruptured and separated, when continental lithosphere is ruptured and separated, when tectonic deformation is localised to form a stable divergent plate boundary, or when decompression melting is established forming oceanic crust; these not being mutually exclusive. The aim of this study is to measure the amount of extension required to generate breakup of the Iberia and Newfoundland margins. This measurement requires the adoption of one of the above definitions of breakup. The definition that lends itself to least ambiguity and measurement error is the rupture and separation of continental crust (i.e. Limit Contiguous Continental Crust, LCCC). As a consequence we measure extension from the proximal margin to the distal limit of contiguous continental crust.

In the case of the Iberia and Newfoundland margins crustal breakup corresponds to the onset of mantle exhumation and separation of continental crust. Therefore this term differs from lithospheric breakup or the onset of steady state sea-floor spreading and hence the formation of a new plate boundary. As shown by Péron-Pinvidic et al., (2007), outboard of thinned contiguous continental crust there may be windows of exhumed mantle followed by continental crustal allochthon blocks on their oceanward side. In 3D these windows of exhumed mantle and continental allochthon blocks are not continuous along strike and anastomose as shown by seismic studies adjacent to the ISE01 and LG12 seismic lines (Péron-Pinvidic et al., 2007; Davy et al., 2018; Lymer et al., 2019).

Figures 4 and 5 summarize the results from gravity anomaly inversion and subsidence analysis for the northern and southern conjugate margin profiles and the locations of these distal limit of contiguous continental crust used to measure extension.

4.1. Distal limit of contiguous continental crust

Cowie et al., (2015) carried out an integrated quantitative analysis consisting of gravity inversion, residual depth anomaly analysis and subsidence analysis on the Western Iberia margin to determine ocean-continent transition structure and continent-ocean boundary location. They successfully showed the importance of using quantitative techniques together with geological observations to determine the continent-ocean architecture of a rifted continental margin. here it exists, we use ODP (Ocean Drilling Program) results to determine the location of the distal limit of contiguous continental crust (LCCC). However, when ODP data does not allow us to unequivocally identify the LCCC, we use the thinning factor ($1\text{-}1/\beta$) obtained from gravity inversion and subsidence analysis together with published seismic interpretations. The thinning factor results from gravity anomaly inversion and subsidence analysis show similar patterns (Figures 4b and 5b), however our preference is to use the thinning factor from the gravity anomaly inversion as it shows a clearer overall trend.

In the case of the Newfoundland margin this approach is not robust enough to allow us to precisely define a unique distal limit of contiguous continental crust. As a consequence we suggest two possible LCCC locations; the inner (LCCC-1) and the outer (LCCC-2) that in turn define the boundaries of a zone within which the location of the LCCC could be placed.

Northern profiles

Along the SCREECH1 seismic profile (Newfoundland margin) there are no ODP well information. Therefore, to define LCCC locations (Figure 4) we use the crustal thinning factor from gravity anomaly inversion (Figure 4b) together with the seismic interpretation suggested by Mohn et al., (2015). We make two estimates of LCCC location. LCCC-1 is located where the “normal” magmatic thinning factor first reaches 1.0. This indicates that complete thinning of continental crust is achieved and thus either exhumed mantle or oceanic crust are present. LCCC-2 is located more distally where the highest value of serpentinized mantle thinning factor occurs which indicates that mantle may be exhumed and thus continental crust is completely thinned. The LCCC-2 location is consistent with the Mohn et

al., (2015) seismic interpretation. Our preference is for LCCC-1 which is consistent with the interpretation of SCREECH1 by Funck et al., (2003).

Along the ISE-01 seismic profile (Iberia margin) ODP well information is available (e.g. Sawyer et al., 1994; Whitmarsh et al., 1998). The ODP Site 639 shows the presence of continental basement, while the ODP Site 637 shows serpentinized peridotite (Figure 4a). The "normal" magmatic thinning factor from gravity anomaly inversion reaches first 1.0 at the western edge of the ODP Site 639 (Figure 4b). This suggests that the distal limit of contiguous continental crust (our LCCC-1 location) may be placed immediately to the west of ODP Site 639. In contrast, the LCCC-2 location is placed at the eastern edge of the ODP Site 637 consistent with the Mohn et al., (2015) seismic interpretation and the Cowie et al., (2015) quantitative analysis.

Southern profiles

Along the SCREECH2 seismic profile (Newfoundland margin), ODP well data is available (Figure 5a). The ODP Site 1276 (Funck et al., 2003) was drilled in "transitional" crust between known continental crust and known oceanic crust. This well shows sills above sediments, however the nature of the basement is uncertain. In contrast, the ODP Site 1277 (Funck et al., 2003) was drilled into a basement high that shows serpentinized peridotite with intrusive and extrusive mafic material interpreted as the onset of steady-state seafloor spreading (see Bronner et al., 2011 for a detailed description). The lack of ODP well information in the proximal margin gives uncertainty on where to place the distal limit of contiguous continental crust along this section. The LCCC-1 location is determined where "normal" magmatic thinning factor first reaches 1.0 (Figure 5b). This is consistent with the seismic interpretation by Mohn et al., (2015). We suggest that the LCCC-2 location may be placed at the western edge of ODP Site 1276 and thus assuming that the known continental crust may terminate before the "transitional" crust identified in this well.

Along the TGS/LG12 seismic profiles (Iberia margin) observations from several ODP drill wells are available (Figure 5a). The ODP Sites1067 and 900 (Whitmarsh et al., 1998; Sawyer et al., 1994) show deep water turbidites over lower crustal rocks (Sutra and Manatschal, 2012; Cowie et al., 2015). In contrast, serpentinized peridotite was drilled at ODP Site 1068 (Whitmarsh et al., 1998), which was interpreted as serpentinized exhumed mantle (Sutra and Manatschal, 2012; Cowie et al., 2015). Given the close proximity between the 1068 and 900 ODP Sites (Figure 5a), we determine the LCCC between these two well positions. Note that

we suggest only a single LCCC location along this section and thus this represents both the inner (LCCC-1) and the outer (LCCC-2) LCCC positions (Figure 5). The thinning factor from gravity anomaly inversion (Figure 5b) can also be used to constrain LCCC location. The analysis by Cowie et al., (2015) along the TGS/LG12 seismic profiles showed that where "normal" magmatic solution of thinning factor first reaches 1.0 corresponds to hyper-extended crust, which extends at least 50 km oceanwards. This is consistent with the LCCC location based on the ODP well data on the TGS/LG12 seismic profile.

4.2. Extension estimates from gravity anomaly inversion and subsidence analysis

Figures 4c and 5c summarize extension estimates along Iberia and Newfoundland conjugate margins obtained by the integration of thinning factor from gravity anomaly inversion and subsidence analysis previously shown in Figures 2 and 3. For completeness, we show the restored bathymetry and Moho depths for the Iberia and Newfoundland conjugate margins at breakup time for the northern (Figure 4d) and southern profiles (Figure 5d). This is achieved by the flexural backstripping of the sediment load and reverse post-rift thermal subsidence modelling (Kusznir et al., 1995; Roberts et al., 1998).

We use the inner and outer LCCC locations previously defined and produce two cross-sections showing the restored Iberia and Newfoundland margins at the continental crustal separation point along the northern (Figure 6) and the southern (Figure 7) profiles. To construct this, we use the restored top basement and Moho horizons between the proximal edge of continental crust and the LCCC locations (Figure 4d and 5d).

Note that to remove the effect of post-breakup uplift on the Newfoundland margin, following earlier discussion, both top-basement and Moho are deepened by 500 m prior to produce the restored bathymetry cross-sections at the time of breakup shown in Figures 6 and 7. A summary of the continental lithosphere extension (from subsidence analysis) and continental crustal extension (from gravity anomaly inversion) required to produce rupture and separation of continental crustis shown in Tables 1-4. The amount of extension that continental lithosphere and continental crust have undergone depends on the LCCC location. The two extension values shown for each quantitative technique correspond to the "normal" magmatic addition and the serpentinized mantle solution used to compute the thinning factor (see section 3.1 for further detail). The averaged values of total continental lithosphere extension and continental crust extension are also shown.

When measuring extension, it is important that the orientation of the profile used is the same as the extension direction. Recently published evidence (Schuba et al., 2018; Lymer et al., 2019) shows that, in the more distal part of the ISE01 seismic profile, the extension direction deviates significantly from the azimuth of the line. However where we determine extension for the contiguous continental crust, we believe that this part of ISE01 is parallel to the extension direction and consequently we are not overestimating crustal extension. It is also important to note that the profiles analysed in this study do not reach the most proximal margins. This is evidenced by the thinning factor being higher than zero at the proximal edge of the seismic lines, except on the ISE01 line. This implies that some proximal extension is missed and that the total extension determined for the SCREECH1, SCREECH2 and TGS/LG12 seismic profiles are minimum estimates.

For crustal breakup to be achieved our measurements for the northern conjugate margin profiles using the LCCC-1 location give extension of 159 km for continental crust and 167 km for continental lithosphere (Table 1). In contrast, using the LCCC-2 location gives continental crust extension of 250 km and continental lithosphere extension of 251 km (Table 2). The results for the southern profiles using the LCCC-1 location show extension of 181 km for continental crust and 194 km for continental lithosphere (Table 3), while using the LCCC-2 location gives extension of 217 km for continental crust and 230 km for continental lithosphere. (Table 4). Our preferred distal limit of contiguous continental crust is LCCC-1 on the evidence of ODP drilling results for the Iberia margin and for the Newfoundland margin supported by the thinning factor profiles from gravity inversion and subsidence analysis.

5. Observed brittle continental crust extension from seismic observations

We determine the observed brittle extension that continental crust has undergone between the proximal edge of continental crust provided by our dataset and its distal end using the inner limit of contiguous continental crust (LCCC-1) defined in section 4.1. To achieve this, we measure the horizontal displacement of the interpreted faults along the northern (Figure 8) and the southern (Figure 9) seismic profiles. Interpretation of seismic data is often non-unique and hence leads to more than one possible geological scenario.

Figure 8b shows the Northern Profiles Seismic Interpretation-1 (NPSI-1) while Figures 9b and 9c show the Southern Profiles Seismic Interpretation-1 (SPSI-1) and the Southern

Profiles Seismic Interpretation-2 (SPSI-2) respectively. The NPSI-1 and SPSI-1 seismic interpretations use classic extensional faults (i.e. steep and planar faults) identified by the offset of the top pre-rift. The NPSI-1 seismic interpretation suggests that brittle continental crust extension of the Newfoundland margin is 36 km while for the Iberia margin it is 84 km (Supplementary material – Table 1-2). In contrast, the SPSI-1 seismic interpretation indicates that brittle continental crust extension of the Newfoundland margin is 48 km while for the Iberia margin it is 71 km (Supplementary material – Table 3-4). Figure 10a shows a classic extensional fault geometry which is typical of continental rifting settings (e.g. Stein and Barrientos, 1985; Jackson, 1987; Roberts and Yielding, 1994). Faults heaves are usually less than 10 km and the lithosphere effective elastic thickness is typically 1.5-3 km for continental rifting (Roberts et al., 1998; White, 1999; Roberts et al., 2019).

The SPSI-2 seismic interpretation is similar to the SPSI-1 seismic interpretation except for part of the Iberia necking domain where a large extensional fault exhumes footwall that is subsequently re-faulted. This interpretation is favoured instead of SPSI-1 which only using steep and planar faults. The SPSI-2 seismic interpretation suggests that the brittle continental crust extension is 89 km for the Iberia margin while 48 km for the Newfoundland margin (Supplementary material – Table 3 and 5). The large extensional fault within the Iberia necking domain in SPSI-2 is consistent with rolling-hinge extensional-type faulting (Buck, 1988) in which a large heave (>10 km) leads to extensive exhumation and flexural isostatic rotation of the footwall block resulting in a sub-horizontal seabed. Figure 10b shows a rolling-hinge extensional-type fault with 20 km of extension and a low lithosphere effective elastic thickness (0.75 km) typically required to form this type of structures.

The NPSI-1 seismic interpretation for the northern Iberia-Newfoundland conjugate margin profiles suggests that the continental crust has undergone 120 km of brittle extension for crustal breakup. In contrast, the two seismic interpretations for the southern Iberia-Newfoundland profiles (SPSI-1 and SPSI-2) indicate 119 km and 137 km of brittle continental crust extension respectively.

6. Fault population analysis to explore sub-seismic faulting

We carry out a fault population analysis to explore whether there may be sub-seismic resolution faulting and if this may significantly contribute to an under-estimation of brittle crustal extension. This analysis determines the proportion of faults which have displacements

too small to be imaged by seismic reflection data (e.g. Walsh et al., 1991; Marrett and Allmendinger, 1992; Gauthier and Lake, 1993; Pickering et al., 1997; Ackerman et al., 2001). Figure 11a shows a generalised example from Ackerman et al., (2001) illustrating the statistical expression of sampling artifacts and cumulative frequency analysis. The sampling artifacts consist of both data censoring because of the limited sampling area and data truncation because of non-imaged faults below the resolution of the seismic reflection data (Pickering et al., 1995). Two cumulative frequency curves are shown (Figure 11a); a power-law distribution that plots as a straight line in log-log space excluding the sampling artifacts and an exponential distribution that plots as a curved line in log-log space including the sampling artifacts. The idealised fault distribution shown by the cumulative frequency analysis consists of a central steep segment with negative gradient representing the average fault population. At large heaves it shows data censoring while for low heaves it shows data truncation (Walsh et al., 1991; Ackerman et al., 2001). The slope of a power-law distribution curve, gives the fractal dimension and is usually between -0.7 and -0.9 suggesting that a proportion of faults are not being seismically observed (Walsh et al., 1991) whereas an exponential distribution type indicates that the majority of faults are being seismically observed (e.g. Ackerman et al., 2001).

Our fault population analysis is carried out using the interpreted faults on the NPSI-1 (Figures 11b-c), SPSI-1 (Figures 11d-e) and SPSI-2 (Figures 11f-g) seismic interpretations to determine the amount of missing extension due to sub-seismic resolution faulting. The distribution of the sampled faults along the northern seismic profiles (NPSI-1 seismic interpretation) apparently fit better with an exponential curve rather than a power-law relationship (Figure 11b-c). However, the relationship distribution between the sampled faults and the exponential curve does not show the same pattern as suggested by Ackerman et al., (2001). Our results show that the central data and truncation data fit perfectly well with the exponential curve while the censoring data is above the predicted frequency curve. The misfit between the data and the exponential distribution curve suggests that a power-law frequency needs to be considered. However, a power-law relationship gives a fractal dimension higher than 1 which is a non-physical solution because this would imply that total extension is greater than the length of the profile. We conclude that the faults sampled along the northern profiles cannot be uniquely represented by either an exponential or power-law distribution frequency and as a consequence we are not able to reliably estimate the amount of sub-seismic faulting. A possible explanation of the fault population results for the northern

profiles, assuming that is not due to an imperfect interpretation of old seismic data, is that there may be two distinct fault populations as suggested by Reston and McDermott 2014. This might arise because rifting within the Galicia Interior Basin is a separate tectonic event occurring several tens of Ma before lithospheric breakup (Jeanniot et al., 2016).

The interpreted faults along the southern seismic profiles (SPSI-1 and SPSI-2 seismic interpretations) show a distribution that matches with a power-law frequency curve (Figures 11d-g). However, the data censoring segment at large heaves does not show the same pattern as suggested by Ackerman et al., (2001), instead the censored data plots above the extrapolated power-law curve rather than below. This may suggest that two distinct fault populations are also present for the southern profiles and/or it may indicate an imperfect interpretation on old seismic data. Despite this, the overall trend of fault data appears to fit with a power-law frequency curve which allows us to obtain the fractal dimension from which the contribution of sub-seismic fault resolution can be determined. Fractal dimension values for the SPSI-1 and SPSI-2 seismic interpretations are -0.8 and -0.7. Following Walsh et al., (1991), these values indicate that between 20-25% of faulting extension is not being seen on the seismic reflection data. Fractal dimensions of -0.8 and -0.7 imply that the measured extension from cumulative fault heave needs to be multiplied by 1.33 and 1.25 respectively to correct for sub-seismic resolution faulting.

7. Discussion

In this section we summarise our results and compare the amount of brittle crustal extension and total continental lithosphere and crustal extension required to produce continental crustal breakup.

7.1. Apparent extension estimates required for crustal breakup

Subsidence analysis, gravity inversion and fault heave summation from seismic observations have been used to determine the amount of extension of continental lithosphere, continental crust and brittle upper crust extension required to produce rupture and separation of continental crust (Figure 12). These measurements have been made between the proximal continental margin and the distal limit of contiguous continental crust (LCCC-1) as defined in this study for the northern and the southern conjugate margins of Iberia and Newfoundland.

Results from quantitative analysis (Tables 1-4) show that continental crust and continental lithosphere were extended by 159 km and 167 km for the northern profiles and 181 km and 194 km for the southern profiles (this is summarised in Figure 12). For each margin the measurements from gravity inversion and subsidence analysis are similar. They indicate that the northern profiles were extended by 163 km and the southern profiles by 187 km to produce rupture and separation of continental crust. This is comparable with the extension estimates of 168 km obtained by Jeanniot et al., (2016), however it is substantially lower than the 242 km proposed by Sutra et al., (2013).

Results from observed fault heave summation based on seismic observations indicate that the brittle continental crust was extended by 120 km using the NPSI-1 seismic interpretation along the northern profiles. For the Iberia margin component of the northern transect using ISE01 we measure 84 km which is slightly greater than the 73 km measured by Reston and McDermott (2014) along the same profile. This difference can be explained because we also include small faults imaged by seismic reflection in our interpretation. For the southern profiles, observed fault extension is 119 km using the SPSI-1 seismic interpretation and 137 km using the SPSI-2 seismic interpretation. Our observed fault extension is also shown for comparison in Figure 12.

Our results show that the seismically observed fault extension is less than the measured extension for the whole continental crust and lithosphere at the scale of the whole conjugate margin system. If material balance is conserved during lithosphere stretching and thinning leading to breakup then we would expect the extension of the brittle continental crust by faulting to be equal to the extension of the continental crust and lithosphere at the scale of the whole conjugate margin system. Figure 12 shows that when observed fault heave summation is compared with lithosphere and crust extension, the former is significantly less than the latter and an apparent extension discrepancy is observed at the scale of the whole conjugate margin system. This extension discrepancy is approximately ~25% for both north and south profiles that we have analysed on the Iberia-Newfoundland conjugate margins.

7.2. Extension estimates required for crustal breakup: including sub-seismic resolution fault

The results from the fault population analysis carried out in this study show that observed fault heaves underestimate the amount of extension by faulting. It is therefore important to include sub-seismic resolution fault extension when comparing fault heave summation with

563 lithosphere and crustal extension. Failing to do so may lead to an apparent extension
564 discrepancy at the scale of the whole conjugate margin system. To correct for sub-seismic
565 resolution faulting, for the southern profiles, each measured fault heave on the SPSI-1
566 interpretation has been multiplied by 1.33 while faults measured on the SPSI-2 seismic
567 interpretation have been multiplied by a factor of 1.25 (see Section 6 for explanation). For the
568 northern profiles, the fault population analysis does not give a meaningful fractal dimension.
569 In order to correct the fault heave summation for the northern profiles for missing fault
570 extension, we multiply the measured faults heaves of interpretation NPSI-1 by 1.33 assuming
571 a similar sub-seismic resolution behaviour as the southern lines in interpretation SPSI-1.

572 The fault heave summations, corrected for sub-seismic resolution faulting, are shown in
573 Figure 12 for comparison with measured extension for continental crust and lithosphere. By
574 including sub-seismic resolution faulting, the corrected fault heave summations are
575 comparable with crust and lithosphere extension values and there is no apparent extension
576 discrepancy.

577 **7.3. The spatial distribution of extension during continental crustal breakup**

578 We examine the spatial distribution of extension for the Iberia-Newfoundland conjugate
579 margins and the relationship between extensional faulting and extension determined from
580 thinning of the continental crust. Figure 13 compares the cumulative fault extension from
581 heave summation together with the cumulative extension from crustal thinning for the north
582 and south Iberia-Newfoundland conjugate margin pairs. For each of the four margins the
583 cumulative extension starts a zero in the proximal regions and increases towards the distal
584 limit of contiguous continental crust. The cumulative fault extension is shown for both
585 observed values and those corrected for sub-seismic resolution faulting. In the case of the
586 south Iberian margin profile, cumulative fault heave is shown for both SPSI-1 and SPSI-2
587 interpretations.

588 Figure 13 shows that while the cumulative extension curves have a similar shape and, when
589 sub-seismic resolution is allowed for, a similar magnitude at the distal limit of contiguous
590 continental crust (LCCC-1), they differ in detail. In places extension from crustal thinning is
591 greater than that from fault heave summation while in other places the opposite occurs. This
592 difference, in particular the difference in slope, allows us to examine the relationship between
593 the distribution of deformation due to upper crustal faulting and that due to lower crustal
594 stretching and thinning. At locations where the gradient of these two curves is the same this

indicates that both the whole continental crust and the brittle continental crust underwent the same amount of extension and therefore depth-uniform lithosphere extension occurred in these areas (see D-U arrow as an example of this in Figure 13). In contrast, at locations where the slope of the two curves differs, this shows that the whole continental crust and the brittle continental crust underwent different amounts of extension across these areas. This implies localised Depth-Dependent Stretching and Thinning (DDST) of the continental lithosphere (e.g. Roberts et al., 1997; Driscoll and Karner, 1998; Davis and Kusznir, 2004; Kusznir and Karner, 2007) at these locations.

Note that DDST may be present in the form of two opposite polarities. We define DDST Polarity-1 as where the cumulative extension from the integrated crustal thinning curve has a greater gradient than the adjusted fault heave summation curve (see DDST-P1 arrow as an example of this in Figure 13). This indicates that the whole continental crust has been more extended than that of the brittle continental crust at a particular location. We define the opposite polarity DDST Polarity-2 where the adjusted fault heave summation curve has a greater gradient than the cumulative extension from integrated crustal thinning curve at a particular location (see DDST-P2 arrow as an example of this in Figure 13). Across the Iberia and Newfoundland margins both localised depth-uniform and depth-dependent stretching and thinning can be seen (Figure 13).

The similarity of the cumulative extension derived from integrated crustal thinning and adjusted fault heave summation at the distal limit of contiguous continental crust of each margin shows that an extension discrepancy at the scale of the whole conjugate margin system is negligible and does not exist.

Northern Profiles

For the northern Newfoundland margin (Figure 13a), the fault heave summation corrected for sub-seismic resolution faulting is 48 km while the cumulative extension derived from integrated crustal thinning is 57 km at the LCCC location. For its conjugate northern Iberia margin (Figure 13a), the fault heave summation corrected for sub-seismic resolution faulting indicates an extension of 111 km while the cumulative extension derived from integrated crustal thinning is 102 km at the LCCC location. For the northern conjugate margin pair, the combined extension of the upper crust by brittle faulting accounting for sub-seismic resolution fault is 159 km and is the same as the 159 km of extension that the whole continental crust underwent. Therefore, there is no extension discrepancy at the scale of the

whole conjugate margin and material balance is conserved (we do accept that the precise matching of these estimates is fortuitous, given the uncertainties involved).

Southern Profiles

For the southern Newfoundland margin, the fault heave summation corrected for sub-seismic resolution fault is 64 km while the cumulative extension derived from integrated crustal thinning is 74 km at the LCCC location (Figure 13b). For the southern Iberia margin, the fault heave summation corrected for sub-seismic resolution faulting curve indicates an extension of 94 km for the SPSI-1 interpretation and 111 km for SPSI-2, while the cumulative extension derived from integrated crustal thinning is 107 km at the LCCC location (Figure 13b). Using the SPSI-1 seismic interpretation, the extension of the crust by brittle faulting accounting for sub-seismic resolution faulting along the southern profiles is 158 km, while using the SPSI-2 it is 175 km. Our preferred seismic interpretation is SPSI-2 which produces a similar extension magnitude to that from gravity inversion, suggesting that the whole continental crust underwent approximately 181 km of extension along the southern profiles. The close similarity of cumulative fault extension and extension from crustal thinning shows no significant difference.

These results indicate, for the northern and southern profiles across the Iberia-Newfoundland conjugate margins that an extension discrepancy between continental crustal thinning and faulting in the brittle continental upper crust does not exist at the scale of the whole conjugate margin system. In addition, it highlights the important role of sub-seismic resolution faulting when estimating extension of the brittle upper crust.

7.4. Depth-dependent stretching and thinning of continental lithosphere

Depth-dependent lithosphere stretching and thinning (DDST) has been observed by many studies in the proximal and necking zone domains of rifted continental margins (see earlier comprehensive references). In addition DDST is predicted by dynamic numerical models of rifted margin formation (e.g. Huismans and Beaumont, 2011; Brune et al. 2014). Figure 14a shows the results of a kinematic “flexural cantilever” model of an advanced intra-continental rift in which extensional faulting of the brittle upper crust is balanced in the lower crust and lithospheric mantle by distributed ductile pure-shear. While upper crustal thinning by faulting is localised, the ductile pure-shear deformation of the lower crust and lithosphere is spread laterally over a wide region; in the case of the model result shown in Figure 14a, the pure-

shear width associated with each fault is 200 km wide. The thinning factor (1-1/β) profile for the ductile pure-shear deformation in the lower crust and mantle is shown in Figure 14b. The formulation and assumptions of the "flexural cantilever" model is described in detail in Kusznir et al., (1991), Kusznir and Ziegler (1992) and Magnavita et al., (1994). The "flexural cantilever" model is a 2D representation of the McKenzie (1978) rift model modified to include flexural isostasy and planar extensional faults.

Figure 14c shows a comparison between the extension profile across the rift derived from crustal thinning and the summation of the fault heaves input into the model shown in Figure 14a. The sensitivity of the extension profile derived from crustal thinning to pure-shear width is examined for pure-shear widths of 100, 200 and 300 km. Note that the total integrated extension is the same for each curve in Figure 14c, it is merely the lateral distribution of the thinning which differs from case to case. We use Figure 14c to discuss the expected pattern of DDST during intra-continental rifting leading to an advanced intra-continental rift prior to hyper-extension.

A rifted continental margin evolves from an intra-continental rift and structural features inherited from early extensional lithosphere deformation are expected to be preserved within a mature margin. While minor regional extensional faulting may extend laterally over many 100s of km in the early stages of intra-continental rifting, mature rift basins become focused and typically have widths of 50-75 km between their major bounding faults (e.g. the Lake Tanganyika Rift, Kusznir and Ziegler, 1992). While the upper continental crust deformation by faulting may be localized within a width of 50-75 km, the deeper distributed ductile pure-shear deformation of the lower continental crust and lithosphere is expected to be much wider (Kusznir et al., 1991). Further extension of this focused rift may eventually lead to necking (Mohn et al., 2012), hyper-extension and the development of a rifted margin.

Therefore within the proximal rifted margin, the legacy of early intra-continental rift basin formation is expected to show crustal thinning with little or no brittle faulting of the upper crust (Figure 14c). Figure 14 shows this within the outboard zones of an intra-continental rift where continental crust is thinned and stretched without significant extensional faulting within the upper crust above. This corresponds to an extreme case of DDST Polarity-1. Within the proximal zones of an advanced intra-continental rift, the normal case of DDST Polarity-1 is also expected (Figure 14c) and is characterized by the gradient of the extension from integrated crustal thinning being greater than the gradient of the cumulative fault heave

curve which indicates that whole crustal extension is greater than that of the brittle continental crust. Roberts et al. (1997) and Davis and Kusznir (2004) provide observations of DDST Polarity-1 from offshore mid-Norway.

In contrast, within the more distal areas of an advanced intra-continental rift, DDST Polarity-2 (the opposite polarity) is expected to occur. This is evidenced by the gradient of the cumulative fault heave curve being greater than the gradient of the extension from integrated crustal thinning suggesting that the brittle upper continental crust is more extended than the whole continental crust.

The simple rift generated model shown in Figure 14 shows a simple symmetric pattern of DDST polarities with Polarity-1 on the proximal edges of the rift and Polarity-2 in the distal centre. In contrast the distribution of DDST polarities shown in Figure 13 based on observations of the Iberia-Newfoundland margins is much more complex. A possible explanation for this observed complexity of DDST polarity may be that continental lithosphere thinning leading to breakup may in its early stages involve several distinct rift sub-basins which grow and merge along strike as breakup is approached.

DDST should not be confused with an extension discrepancy at the scale of the whole conjugate margin system. However despite of DDST being expected at proximal rifted margins, depth uniform stretching and thinning may occur in the early stages of rifting as observed in the Corinth Rift (Central Greece) and the Halten Terrace (offshore mid Norway) (e.g. Bell et al., 2011; Bell et al., 2014 and references therein).

7.5. Uncertainties on determining brittle fault extension

When determining whether a discrepancy between the observed fault heave summation and lithosphere/crust extension at the scale of the whole conjugate system exists or not, two uncertainties should be addressed; (i) fault geometries and (ii) the distal limit of contiguous continental crust location.

Fault geometries

Interpretation of seismic data is often non-unique and may lead to more than one interpreted geological scenario. For the southern profiles of Iberia and Newfoundland conjugate margins, two seismic interpretations have been proposed. Results from fault heave summation using only planar faults (SPSI-1) or a large rolling-hinge fault and planar faults (SPSI-2) provide

substantially different amounts of observed brittle crustal extension (Figure 12). The interpretation of rolling-hinge faults increases the amount of brittle crustal extension and therefore failing to recognize them may lead to an apparent extension discrepancy at the scale of the whole conjugate margin system. Our preferred seismic interpretation is SPSI-2, as pointed out above, and emphasizes the importance of rolling-hinge extensional faults within the necking zones of rifted margins where continental crust is thinned from 25 km thick to approximately 10 km (Tugend et al., 2014). How this extreme thinning occurs is a current debated topic but the presence of rolling-hinge faults may play an important role during the necking rifting stage (e.g. Mohn et al., 2012).

Results from the fault population analysis show that the overall trend of faults sampled along the southern profiles appears to fit with a power-law frequency curve, however, an unexpected pattern at large fault heaves is observed (Figure 11). This unexpected pattern, where censored data clearly plots above rather than below the extrapolated power-law line, may indicate the presence of two or more fault populations. These populations could correspond to; (i) the presence of two types of fault geometries (planar and rolling-hinge) and/or (ii) two different fault coupling levels (i.e. faults decoupled from and coupled into the mantle).

The fault population statistics for the northern profiles, cannot be represented with a unique frequency curve, which may also indicate the presence of two or more fault populations. Faulting within the older Galicia Interior Basin is expected to be decoupled from the mantle while the younger faulting associate with the lithospheric breakup is expected to be both decoupled and coupled into the mantle. An alternative explanation, discussed earlier, is that the Galicia interior Basin represents a distinct earlier rift not related to breakup.

Distal limit of contiguous continental crust location

Accurately determining the precise location of continental breakup can be difficult and as a consequence two possible LCCC positions have been proposed in this study which in turn define the boundaries of a zone within which the location of the LCCC could be placed. To measure lithosphere and crust extension as well as fault heave summation from seismic data we use the LCCC-1 location as the distal end of continental crust. The observed cumulative fault heave summation corrected for sub-seismic faulting and the integrated extension from crustal thinning match well at the LCCC-1 location for the Iberia profiles (Figure 13). This is consistent with mass conservation during lithosphere stretching and thinning leading to

752 breakup. If mass is conserved during extension, then we would presume the brittle
753 continental crust extension (i.e. extensional faulting) and the whole continental crust
754 extension (i.e. extensional faulting and deeper distributed pure-shear deformation) to be the
755 same.

756 7.6. Alternative processes that may occasionally generate an apparent extension
757 discrepancy

758 Alternative processes that might generate an apparent extension discrepancy at the scale of
759 the whole conjugate margin are non-brittle extension and continued thinning of continental
760 crust after rupture and separation of continental crust.

761 Non-brittle extension might be achieved through either dyking (extremely rare at magma-
762 poor rifted margins) or non-brittle plastic deformation (Davis and Kusznir, 2004), but it has
763 been suggested that the majority of upper continental crust deformation is accommodated by
764 seismic slip on faults (Jackson and McKenzie, 1983; Jackson, 1987). An alternative
765 possibility is that continental crust may be extended after continental crustal breakup occurs.
766 This might be achieved by deeper ductile lithosphere deformation associated with extensional
767 faulting within exhumed continental mantle, however how this could be recognized is
768 uncertain. Polyphase faulting has been proposed consisting of new faults cutting across
769 existing back-rotated and abandoned fault systems leading to complex fault geometries,
770 which are difficult to recognize on seismic data (e.g. Reston 2005; Reston and McDermott,
771 2014). Re-faulting of exhumed fault footwall, however, can be observed within our
772 interpretation (Figure 9) and is accounted for in the fault heave summation in this study.
773 Measured fault extension corrected for sub-seismic resolution faulting and its close
774 agreement with extension measure from the thinning of continental crust and lithosphere on
775 the Iberia-Newfoundland margins, suggests that these additional mechanisms are not required
776 to match extension from crustal and lithosphere thinning.

777 8. Conclusions

778 This study aims to determine, for the conjugate Iberia-Newfoundland rifted margins, the
779 extension required to produce continental crustal breakup defined as when continental crustal
780 rupture and separation occurs. We measure extension from the proximal margin to the distal
781 limit of contiguous continental crust by integrating the thinning of continental crust and
782 lithosphere, measured by gravity inversion and subsidence analysis, and by summing

783 extensional fault heaves interpreted from seismic reflection data and corrected for sub-
784 seismic resolution faulting. The key conclusions are the following:

785 1- To achieve crustal breakup across the conjugate Iberia-Newfoundland margins, we
786 estimate that approximately 172 km of extension are required. An appropriate follow-
787 up to this study would be to test the applicability of this value to other conjugate
788 margins of both similar and dissimilar type.
789 2- An apparent extension discrepancy at the scale of the whole conjugate margin system
790 is seen when seismically observed fault heave summation is compared with extension
791 from crust and lithosphere thinning, the former being ~25% less than the latter.
792 3- Allowing for fault extension at sub-seismic resolution, an extension discrepancy at the
793 scale of the whole conjugate Iberia-Newfoundland margin system is shown not to
794 exist.
795 4- In addition to sub-seismic faulting, fault geometries and the location of the distal limit
796 of contiguous continental crust are important issues that need to be carefully
797 considered when comparing estimates from fault heave summation and extension
798 from crust and lithosphere thinning.
799 5- Failing to recognize rolling-hinge faults may lead to an under-estimate of fault
800 extension.
801 6- Depth-dependent stretching and thinning (DDST Polarity-1 and Polarity-2) is
802 observed and expected at rifted margins. Localised DDST should not be confused
803 with an extension discrepancy at the scale of the whole conjugate margin system.

804 We believe that our results for the Iberia-Newfoundland conjugate margins example may
805 provide insights towards a better understanding of continental crustal breakup at other
806 conjugate rifted margins.

807 ## Acknowledgments

808 We acknowledge the MM4 (Margin Modelling Phase 4) industry partners (BP,
809 ConocoPhillips, Statoil, Petrobras, Total, Shell, BHP-Billiton, and BG) for financial support
810 and discussions. We thank Garry Karner, Robert Hooper, Rebecca Bell and Pablo J.
811 González, for fruitful discussions.

812

REFERENCES

Ackermann, R. V, Schlische, R.W., Withjack, M.O., 2001. The geometric and statistical evolution of normal fault systems: an experimental study of the effects of mechanical layer thickness on scaling laws. J. Struct. Geol. 23, 1803–1819.

Alves, T.M., Cunha, T., 2018. A phase of transient subsidence, sediment bypass and deposition of regressive–transgressive cycles during the breakup of Iberia and Newfoundland. Earth Planet. Sci. Lett. 484, 168–183.

Alvey, A., Gaina, C., Kusznir, N.J., Torsvik, T.H., 2008. Integrated crustal thickness mapping and plate reconstructions for the high Arctic. Earth Planet. Sci. Lett. 274, 310–321. https://doi.org/10.1016/j.epsl.2008.07.036.

Baxter, K., Cooper, G.T., Hill, K.C., O'Brien, G.W., 1999. Late Jurassic subsidence and passive margin evolution in the Vulcan Sub-basin, north-west Australia: Constraints from basin modelling. Basin Res. 11, 97–111. https://doi.org/10.1046/j.1365-2117.1999.00088.

Bell, R.E., Mcneill, L.C., Henstock, T.J., Bull, J.M., 2011. Comparing extension on multiple time and depth scales in the Corinth Rift , Central Greece. Geophys. J. Int. 186, 463–470. https://doi.org/10.1111/j.1365-246X.2011.05077.

Bell, R.E., Jackson, C.A., Elliott, G.M., Gawthorpe, R.L., Sharp, I.R., Michelsen, L., 2014. Insights into the development of major rift-related unconformities from geologically constrained subsidence modelling: HaltenTerrace, offshore mid Norway. Basin Res. 26, 203–224. https://doi.org/10.1111/bre.12049.

Beslier, M.O., 1996. Data report: Seismic line LG12 in the Iberia Abyssal Plain in Whitmarsh, R.B., Sawyer, D.S., Klaus, A., and Masson, D.G. (Eds.). Proc. Ocean Drill. Program, Sci. Results 149, 737–739.

Bronner, A., Sauter, D., Manatschal, G., Péron-Pinvidic, G., Munschy, M., 2011. Magmatic breakup as an explanation for magnetic anomalies at magma-poor rifted margins. Nat. Geosci. 4, 461–461.

Brune, S., Popov, A.A., Sobolev, S. V., 2012. Modeling suggests that oblique extension facilitates rifting and continental break-up. J. Geophys. Res. Solid Earth 117, 1–16. https://doi.org/10.1029/2011JB008860.

Brune, S., Heine, C., Pérez-Gussinyé, M., Sobolev, S. V, 2014. Rift migration explains continental margin asymmetry and crustal hyper-extension. Nat. Commun. 5, 4014. https://doi.org/10.1038/ncomms5014.

Buck, W.R., 1988. Flexural Rotation of Normal Faults. Tectonics 7, 959–973.

Cannat, M., Manatschal, G., Sauter, D., Péron-Pinvidic, G., 2009. Assessing the conditions of continental breakup at magma-poor rifted margins: What can we learn from slow spreading mid-ocean ridges? Comptes Rendus - Geosci. 341, 406–427.

Carlson, R.L., Herrick, C.N., 1990. Densities and porosities in the oceanic crust and their variations with depth and age. J. Geophys. Res. 95, 9153–9170. https://doi.org/10.1029/JB095iB06p09153.

Chappell, A.R., Kusznir, N.J., 2008. Three-dimensional gravity inversion for Moho depth at rifted continental margins incorporating a lithosphere thermal gravity anomaly correction. Geophys. J. Int. 174, 1–13. https://doi.org/10.1111/j.1365-246X.2008.03803.

Chian, D., Louden, K.E., Minshull, T.A., Whitmarsh, R.B., 1999. Deep structure of the ocean-continent transition in the southern Iberia Abyssal Plain from seismic refraction profiles : Ocean Drilling Program (Legs 149 and 173) transect Deping Chian seismic refraction of an 80x40 of the southern reflection / refracti 104, 7443–7462.

Christensen, N.I., Mooney, W.D., 1995. Seismic velocity structure and composition of the continental crust: a global view. J. Geophys. Res. 100, 9761–9788. https://doi.org/10.1029/95JB00259.

Cowie, L., Kusznir, N., Manatschal, G., 2015. Determining the COB location along the Iberian margin and Galicia Bank from gravity anomaly inversion, residual depth anomaly and subsidence analysis. Geophys. J. Int. 203, 1355–1372. https://doi.org/10.1093/gji/ggv367

Crosby, A., White, N., Edwards, G., Shillington, D.J., 2008. Evolution of the Newfoundland – Iberia conjugate rifted margins. Earth Planet. Sci. Lett. 273, 214–226. https://doi.org/10.1016/j.epsl.2008.06.039.

Davis, M., Kusznir, N., 2004. Depth-dependent lithospheric stretching at rifted continental margins. In: Karner, G.D. (ed). Proc. NSF Rift. Margins Theor. Institute. Columbia Univ. Press. New York 92–136. https://doi.org/10.7312/karn12738-005.

873 Davy, R.G., Minshull, T.A., Bayrakci, G., Bull, J.M., Klaeschen, D., Papenberg, C., Reston,
874 T.J., Sawyer, D.S., Zelt, C.A., 2016. Continental hyperextension, mantle exhumation,
875 and thin oceanic crust at the continent-ocean transition, West Iberia: New insights from
876 wide-angle seismic. J. Geophys. Res. Solid Earth 767–787.

877 Davy, R.G., Morgan, J. V., Minshull, T.A., Bayrakci, G., Bull, J.M., Klaeschen, D., Reston,
878 T.J., Sawyer, D.S., Lymer, G., Cresswell, D., 2018. Resolving the fine-scale velocity
879 structure of continental hyperextension at the Deep Galicia Margin using full-waveform
880 inversion. Geophys. J. Int. 212, 244–263. https://doi.org/10.1093/gji/ggx415

881 Divins, D.L., 2003. Total Sediment Thickness of the World's Oceans and Marginal Seas.
882 NOAA Natl. Geophyisical Data Center, Boulder, CO.

883 Driscoll, N.W., Karner, G.D., 1998. Lower crustal extension across the Northern Carnarvon
884 basin, Australia: Evidence for an eastward dipping detachment. J. Geophys. Res. 103,
885 4975–4991.

886 Eddy, M.P., Jagoutz, O., Ibañez-Mejia, M., 2017. Timing of initial seafloor spreading in the
887 Newfoundland-Iberia rift. Geology 45, 527–530.
888 https://doi.org/10.1130/G38766.1Funck, T., Hopper, J.R., Larsen, H.C., Louden, K.E.,
889 Tucholke, B.E., Holbrook, W.S., 2003. Crustal structure of the ocean-continent
890 transition at Flemish Cap : Seismic refraction results. J. Geophys. Res. 108, 2531.
891 https://doi.org/10.1029/2003JB002434.

892 Gauthier, B.D.M., Lake, S.D., 1993. Probabilistic modeling of faults below the limit of
893 seismic resolution if Pelican Field, North Sea, Offshore United Kingdom. Am. Assoc.
894 Pet. Geol. Bull. 77, 761–777.

895 Gillard, M., Sauter, D., Tugend, J., Tomasi, S., Epin, M.-E., Manatschal, G., 2017. Birth of
896 an oceanic spreading center at a magma-poor rift system. Sci. Rep. 7.
897 https://doi.org/10.1038/s41598-017-15522-2.

898 Gozzard, S., Kusznir, N., Franke, D., Cullen, A., Reemst, P., Henstra, G., 2018. South China
899 Sea crustal thickness and oceanic lithosphere distribution from satellite gravity
900 inversion. Pet. Geosci. https://doi.org/https://doi.org/10.1144/petgeo2016-162.

901 Grevemeyer, I., Ranero, C.R., Ivandic, M., 2018. Structure of oceanic crust and
902 serpentinization at subduction trenches. Geosphere 14, 395–418.

https://doi.org/10.1130/GES01537.1

Grevemeyer, I., Ranero, C.R., Ivandic, M., 2018. Structure of oceanic crust and serpentinization at subduction trenches. Geosphere. 14 (2): 395-418.

Haupert, I., Manatschal, G., Decarlis, A., Unternehr, P., 2016. Upper-plate magma-poor rifted margins: Stratigraphic architecture and structural evolution. Mar. Pet. Geol. 69, 241–261. https://doi.org/10.1016/j.marpetgeo.2015.10.020.

Huismans, R., Beaumont, C., 2011. Depth-dependent extension, two-stage breakup and cratonic underplating at rifted margins. Nature 473, 74–78.

Huismans, R.S., Beaumont, C., 2014. Rifted continental margins: The case for depth-dependent extension. Earth Planet. Sci. Lett. 407, 148–162. https://doi.org/10.1016/j.epsl.2014.09.032.

Jackson, J., McKenzie, D., 1983. The geometrical evolution of normal fault systems. J. Struct. Geol. 5, 471–482. https://doi.org/10.1016/0191-8141(83)90053-6.

Jackson, J., 1987. Active normal faulting and crustal extension. Geol. Soc. London, Spec. Publ. 28, 3–17. https://doi.org/10.1144/GSL.SP.1987.028.01.02.

Jeanniot, L., Kusznir, N., Mohn, G., Manatschal, G., Cowie, L., 2016. Constraining lithosphere deformation modes during continental breakup for the Iberia-Newfoundland conjugate rifted margins. Tectonophysics 680, 28–49. https://doi.org/10.1016/j.tecto.2016.05.006.

Jordan, T.H., Anderson, D.L., 1974. Earth Structure from Free Oscillations and Travel Times. Geophys. J. R. Astron. Soc. 36, 411–459. https://doi.org/10.1111/j.1365-246X.1974.tb03648.

Kusznir, N.J., Marsden, G., Egan, S.S., 1991. A flexural-cantilever simple-shear/pure-shear model of continental lithosphere extension: applications to the Jeanne d'Arc Basin, Grand Banks and Viking Graben, North Sea. Geol. Soc. London, Spec. Publ. 56, 41–60. https://doi.org/10.1144/gsl.sp.1991.056.01.04.

Kusznir, N.J., Ziegler, P.A., 1992. The mechanics of continental extension and sedimentary basin formation : A simple-shear / pure-shear flexural cantilever model. Tectonophysics

215, 117–131.

Kusznir, N.J., Roberts, A.M., Morley, C.K., 1995. Forward and reverse modelling of rift basin formation. Geol. Soc. London, Spec. Publ. 80, 33–56. https://doi.org/10.1144/gsl.sp.1995.080.01.02.

Kusznir, N.J., Hunsdale, R., Roberts, A.M., 2004. Timing of depth-dependent lithosphere stretching on the S. Lofoten rifted margin offshore mid-Norway: Pre-breakup or post-breakup? Basin Res. 16, 279–296. https://doi.org/10.1111/j.1365-2117.2004.00233.

Kusznir, N.J., Karner, G.D., 2007. Continental lithospheric thinning and breakup in response to upwelling divergent mantle flow: application to the Woodlark, Newfoundland and Iberia margins. Geol. Soc. London, Spec. Publ. 282, 389–419. https://doi.org/10.1144/SP282.16.

Kusznir, N.J., Roberts, A.M., Alvey, A.D., 2018. Crustal structure of the conjugate Equatorial Atlantic Margins, derived by gravity anomaly inversion. Geol. Soc. London, Spec. Publ. SP476.5. https://doi.org/10.1144/sp476.5.

Lymer, G., Cresswell, D.J.F., Reston, T.J., Bull, J.M., Sawyer, D.S., Morgan, J.K., Stevenson, C., Causer, A., Minshull, T.A., Shillington, D.J., 2019. 3D development of detachment faulting during continental breakup. Earth Planet. Sci. Lett. 515, 90–99. https://doi.org/10.1016/j.epsl.2019.03.018.

Magnavita, L.P., Davison, I., Kusznir, N.J., 1994. Rifting, erosion, and uplift history of the Reconcavo-Tucano-Jatoba Rift, northeast Brazil. Tectonics 13, 367–388.Manatschal, G., 2004. New models for evolution of magma-poor rifted margins based on a review of data and concepts from West Iberia and the Alps. Int. J. Earth Sci. 93, 432–466. https://doi.org/10.1007/s00531-004-0394-7.

Marrett, R., Allmendinger, R.W., 1992. Amount of extension on “small’’ faults: an example from the Viking graben.” Geology 20, 47–50.

Mckenzie, D., 1978. Some Remarks on Development of Sedimentary Basins. Earth Planet. Sci. Lett. 40, 25–32.

Mohn, G., Manatschal, G., Beltrando, M., Masini, E., Kusznir, N., 2012. Necking of continental crust in magma-poor rifted margins: Evidence from the fossil Alpine Tethys margins. Tectonics 31, 1–28. https://doi.org/10.1029/2011TC002961.

962 Mohn, G., Karner, G., Manatschal, G., Johnson, C., 2015. Structural and stratigraphic
963 evolution of the Iberia and Newfoundland hyper-extended rifted margins: A quantitative
964 modeling approach. Sediment. Basin Crustal Process. Cont. Margins From Mod. Hyper-
965 extended Margins to Deform. Anc. Analog. 16, 9156. https://doi.org/10.1144/SP413.9.

966 Müller, R.D., Sdrolias, M., Gaina, C., Roest, W.R., 2008. Age, spreading rates, and spreading
967 asymmetry of the world's ocean crust. Geochemistry, Geophys. Geosystems 9, 1–19.
968 https://doi.org/10.1029/2007GC001743.

969 Parker, R.L., 1972. The rapid calculation of potential anomalies. Geophys. J. R. Astron. Soc.
970 31, 447–455.

971 Péron-Pinvidic, G., Manatschal, G., Minshull, T.A., Sawyer, D.S., 2007. Tectonosedimentary
972 evolution of the deep Iberia-Newfoundland margins: Evidence for a complex breakup
973 history. Tectonics 26, 1–19. https://doi.org/10.1029/2006TC001970.

974 Pickering, G., Bull, J.M., Sanderson, D.J., 1995. Sampling power-law distributions.
975 Tectonophysics 248, 1–20. https://doi.org/10.1016/0148-9062(96)80040-4.

976 Pickering, G., Peacock, D.C.P., Sanderson, D.J., Bull, J.M., 1997. Modeling Tip Zones to
977 Predict the Throw and Length Characteristics of Faults. Am. Assoc. Pet. Geol. Bull. 81.

978 Ranero, C.R., Pérez-Gussinyé, M., 2010. Sequential faulting explains the asymmetry and
979 extension discrepancy of conjugate margins. Nature 468, 294–299.
980 https://doi.org/10.1038/nature09520.Reston, T.J., 2005. Polyphase faulting during the
981 development of the west Galicia rifted margin. Earth Planet. Sci. Lett. 237, 561–576.
982 https://doi.org/10.1016/j.epsl.2005.06.019.

983 Reston, T., McDermott, K., 2014. An assessment of the cause of the "extension discrepancy"
984 with reference to the west Galicia margin. Basin Res. 26, 135–153.
985 https://doi.org/10.1111/bre.12042.

986 Roberts, A.M., Yielding, G., 1994. Continental Extensional Tectonics. In: Hancock, P.L.
987 (ed.) Continental Deformation, Pergamon Press, 223-250.

988 Roberts, A.M., Lundin, E.R., Kusznir, N.J., 1997. Subsidence of the Vøring Basin and the
989 influence of the Atlantic continental margin. J. Geol. Soc. London 154, 551–557.
990 https://doi.org/10.1144/gsjgs.154.3.0551.

991 Roberts, A.M., Kusznir, N.J., Yielding, G., Styles, P., 1998. 2D flexural backstripping of

992 extensional basin: the need for a sideways glance. Pet. Geosci. 4, 327–338.
993 https://doi.org/10.1144/petgeo.4.4.327.

994 Roberts, A.M., Kusznir, N.J., Corfield, R.I., Thompson, M., Woodfine, R., 2013. Integrated
995 tectonic basin modelling as an aid to understanding deep-water rifted continental margin
996 structure and location. Pet. Geosci. 19. https://doi.org/10.1144/petgeo2011-046.

997 Roberts, A.M., Alvey, A.D., Kusznir, N.J., 2018. Crustal structure and heat-flow history in
998 the UK Rockall Basin , derived from backstripping and gravity-inversion analysis. Pet.
999 Geosci. https://doi.org/https://doi.org/10.1144/petgeo2017-063.

1000 Roberts, A.M., Kusznir, N.J., Yielding, G., Beeley, H., 2019. Mapping the bathymetric
1001 evolution of the northern North Sea: from Jurassic syn-rift archipelago through
1002 Cretaceous-Tertiary post-rift subsidence. Pet. Geosci.

1003 Russell, S.M., Whitmarsh, R.B., 2003. Magmatism at the west Iberia non-volcanic rifted
1004 continental margin: Evidence from analyses of magnetic anomalies. Geophys. J. Int.
1005 154, 706–730. https://doi.org/10.1046/j.1365-246X.2003.01999.

1006 Sandwell, D.T., Smith, W.H.F., 2009. Global marine gravity from retracked Geosat and ERS-
1007 1 altimetry: Ridge segmentation versus spreading rate. J. Geophys. Res. Solid Earth 114,
1008 1–18. https://doi.org/10.1029/2008JB006008.

1009 Sawyer, D.S., Whitmarsh, R.B., Klaus, A., Party, S.S., 1994. Proceedings of the Ocean
1010 Drilling Program, Initital Repts., 149,. Coll. Station. TX (Ocean Drill. Program).

1011 Schuba, C.N., Gray, G.G., Morgan, J.K., Sawyer, D.S., Shillington, D.J., Reston, T.J., Bull,
1012 J.M., Jordan, B.E., 2018. A low-angle detachment fault revealed: Three-dimensional
1013 images of the S-reflector fault zone along the Galicia passive margin. Earth Planet. Sci.
1014 Lett. 492, 232–238. https://doi.org/10.1016/j.epsl.2018.04.012.Sclater, J.G., Christie,
1015 P.A.F., 1980. Continental stretching: an explanation of the post-mid-Cretaceous
1016 subsidence of the central North Sea Basin. J. Geophys. Res. 85, 3711–3739.

1017 Shillington, D.J., Holbrook, W.S., Van Avendonk, H.J.A., Tucholke, B.E., Hopper, J.R.,
1018 Louden, K.E., Larsen, H.C., Nunes, G.T., 2006. Evidence for asymmetric nonvolcanic
1019 rifting and slow incipient oceanic accretion from seismic reflection data of the
1020 Newfoudland margin. J. Geophys. Res. Solid Earth 111.
1021 https://doi.org/10.1029/2005JB003981.

1022 Smith, R.A., 1961. A uniqueness theorem concerning gravity fields. Math. Proc. Cambridge
1023 Philos. Soc. 57, 865–870.

1024 Smith, W.H., Sandwell, D., 1997. Global sea floor topography from satellite altimetry and
1025 ship depth soundings. Science (80-.). 277, 1956–1962.

1026 Soares, D.M., Alves, T.M., Terrinha, P., 2012. The breakup sequence and associated
1027 lithospheric breakup surface: Their significance in the context of rifted continental
1028 margins (West Iberia and Newfoundland margins, North Atlantic). Earth Planet. Sci.
1029 Lett. 355–356, 311–326. https://doi.org/10.1016/j.epsl.2012.08.036.

1030 Stein, R.-S., Barrientos, S.-E., 1985. Planar High-Angle Faulting in the Basin and Range:
1031 Geodetic Analysis of the 1983 Borah Peak, Idaho, Earthquake. J. Geophys. Res. 90,
1032 11,355-11,366.

1033 Steinberger, B., Conrad, C.P., Osei Tutu, A., Hoggard, M.J., 2017. On the amplitude of
1034 dynamic topography at spherical harmonic degree two. Tectonophysics 760, 221–228.
1035 https://doi.org/10.1016/j.tecto.2017.11.032.

1036 Sutra, E., Manatschal, G., 2012. How does the continental crust thin in a hyperextended rifted
1037 margin? Insights from the iberia margin. Geology 40, 139–142.
1038 https://doi.org/10.1130/G32786.1.

1039 Sutra, E., Manatschal, G., Mohn, G., Unternehr, P., 2013. Quantification and restoration of
1040 extensional deformation along the Western Iberia and Newfoundland rifted margins.
1041 Geochemistry, Geophys. Geosystems 14, 2575–2597.

1042 Tugend, J., Manatschal, G., Kusznir, N.J., Masini, E., 2014. Characterizing and identifying
1043 structural domains at rifted continental margins: application to the Bay of Biscay
1044 margins and its Western Pyrenean fossil remnants. Geological Society, London, Special
1045 Publications, 413.10.1144/SP413.3.

1046 Van Avendonk, H.J.A., Holbrook, W.S., Nunes, G.T., Shillington, D.J., Tucholke, B.E.,
1047 Louden, K.E., Larsen, H.C., Hopper, J.R., 2006. Seismic velocity structure of the rifted
1048 margin of the eastern Grand Banks of Newfoundland , Canada 111, 1–26.
1049 https://doi.org/10.1029/2005JB004156.Walsh, J., Watterson, J., Yieldingt, G., 1991. The
1050 importance of small-scale faulting in regional extension. Nature 351.

1051 White, R., McKenzie, D., 1989. Magmatism at Rift Zones - the Generation of Volcanic

Continental Margins and Flood Basalts. J. Geophys. Res. Earth Planets 94, 7685–7729.

White, R.S., 1999. The lithosphere under stress. Philos. Trans. R. Soc. A Math. Phys. Eng. Sci. 357, 901–915. https://doi.org/10.1098/rsta.1999.0357.

Whitmarsh, R.B., 1998. Proceedings of the Ocean Drilling Program, Initial Reports, vol. 173, Ocean Drill. Program, College Station, Tex.

Zelt, C.A., Sain, K., Naumenko, J. V, Sawyer, D.S., 2003. Assessment of crustal velocity models using seismic refraction and reflection tomography. Geophys. J. Int. 609–626.

TABLES

	Extension SCREECH-1	Extension ISE-01	Total Extension (IB-NF)
Continental crust (GI)	**56-58 km**	**102-103 km**	**159 km**
Continental lithosphere (SA)	**61-63 km**	**104-105 km**	**167 km**

Table 1: Continental crust extension (GI: Gravity Inversion) and continental lithosphere extension (SA: Subsidence Analysis) required to produce crustal breakup using the LCCC-1 location along the northern profiles.

1097

1098

	Extension SCREECH-1	Extension ISE-01	Total Extension (IB-NF)
Continental crust (GI)	**99-106 km**	**145-150 km**	**250 km**
Continental lithosphere (SA)	**101-109 km**	**144-148 km**	**251 km**

Table 2: Continental crust extension (GI: Gravity Inversion) and continental lithosphere extension (SA: Subsidence Analysis) required to produce crustal breakup using the LCCC-2 location along the northern profiles.

1099

1100

1101

1102

1103

1104

1105

1106

1107

1108

1109

1110

1111

1112

1113

1114

1115

	Extension SCREECH-2	Extension TGS/LG12	Total Extension (IB-NF)
Continental crust (GI)	**74-75 km**	**103-110 km**	**181 km**
Continental lithosphere (SA)	**77-78 km**	**114-120 km**	**194 km**

Table 3: Continental crust extension (GI: Gravity Inversion) and continental lithosphere extension (SA: Subsidence Analysis) required to produce crustal breakup using the LCCC-1 location along the southern profiles.

	Extension SCREECH-2	Extension TGS/LG12	Total Extension (IB-NF)
Continental crust (GI)	**109-113 km**	**103-110 km**	**217 km**
Continental lithosphere (SA)	**110-116 km**	**114-120 km**	**230 km**

Table 4: Continental crust extension (GI: Gravity Inversion) and continental lithosphere extension (SA: Subsidence Analysis) required to produce crustal breakup using the LCCC-2 location along the southern profiles.

ELECTRONIC SUPPLEMENT

Northern Profile Seismic Interpretation-1 (Newfoundland)		
Faults numbers	**Faults heaves (km)**	**Total extension (km)**
1	1.9	**36**
2	1.6	
3	0.8	
4	0.3	
5	0.3	
6	0.5	
7	0.7	
8	0.8	
9	0.6	
10	2.2	
11	0.7	
12	1.9	
13	3.1	
14	2.1	
15	3.7	
16	0.8	
17	4.6	
18	0.8	
19	0.3	
20	1.9	
21	1.4	
22	1.5	
23	1.2	
24	1.3	
25	0.9	

Supplementary Table 1: Horizontal faults heaves for the Newfoundland northern profile using the NPSI-1. Fault number 1 is the more proximal one.

Northern Profile Seismic Interpretation-1 (Iberia)		
Faults numbers	**Faults heaves (km)**	**Total extension (km)**
1	7.7	**84**
2	0.4	
3	5.8	
4	1.4	
5	0.9	
6	1.5	
7	1.4	
8	0.3	
9	0.4	
10	1.9	
11	0.3	
12	0.3	
13	0.4	
14	0.6	
15	1.3	
16	1.0	
17	0.7	
18	0.7	
19	1.2	
20	0.3	
21	0.9	
22	1.2	
23	0.8	
24	0.6	
25	0.3	
26	0.4	
27	0.2	
28	0.1	

29	1.0
30	0.7
31	1.2
32	0.9
33	1.9
34	0.7
35	0.2
36	1.4
37	0.5
38	1.0
39	0.5
40	0.8
41	0.6
42	0.4
43	1.9
44	0.5
45	0.5
46	0.5
47	1.6
48	0.5
49	0.5
50	0.3
51	0.4
52	0.4
53	0.7
54	0.9
55	0.6
56	0.9
57	0.3
58	0.4
59	0.2

60	0.4
61	0.7
62	0.4
63	1.6
64	0.8
65	1.4
66	3.9
67	3.6
68	0.9
69	5.1
70	0.5
71	2.9
72	0.9
73	0.8
74	4.3

Supplementary Table 2: Horizontal faults heaves for the Iberia northern profile using the NPSI-1. Fault number 1 is the more proximal one.

Southern Profile Seismic Interpretation-1 & 2 (Newfoundland)		
Faults numbers	**Fault heaves (km)**	**Total extension (km)**
1	0.5	**48**
2	0.4	
3	0.2	
4	2.4	
5	0.6	
6	0.7	
7	1.2	
8	0.4	
9	0.2	
10	2.1	
11	0.3	
12	0.7	
13	0.7	
14	0.3	
15	0.7	
16	0.7	
17	6.5	
18	0.9	
19	0.7	
20	0.4	
21	0.7	
22	0.7	
23	1.6	
24	1.0	
25	7.3	
26	1.7	
27	0.7	
28	0.9	

29	0.3
30	0.3
31	0.5
32	0.4
33	0.4
34	2.0
35	7.3
36	0.6
37	1.0
38	0.4

Supplementary Table 3: Horizontal faults heaves for the Newfoundland southern profile using the SPSI-1 and SPSI-2. Fault number 1 is the more proximal one.

Southern Profile Seismic Interpretation-1 (Iberia)		
Faults numbers	**Faults heaves (km)**	**Total extension (km)**
1	10.9	**71**
2	6.5	
3	0.4	
4	1.1	
5	0.5	
6	6.9	
7	0.2	
8	0.2	
9	1.4	
10	1.1	
11	1.0	
12	0.7	
13	1.3	
14	2.0	
15	0.6	
16	1.3	
17	0.8	
18	6.4	
19	1.6	
20	0.9	
21	0.5	
22	0.5	
23	0.3	
24	6.8	
25	0.5	
26	0.4	
27	1.4	
28	6.8	

	29	4.5	
	30	3.4	
	31	0.3	

Supplementary Table 4: Horizontal faults heaves for the Iberia southern profile using the SPSI-1. Fault number 1 is the more proximal one.

Southern Profile Seismic Interpretation-2 (Iberia)		
Faults Numbers	**Faults heaves (km)**	**Total extension (km)**
1	10.9	**89**
2	6.5	
3	0.4	
4	1.1	
5	0.5	
6	6.9	
7	0.2	
8	0.2	
9	34.7	
10	1.6	
11	0.9	
12	0.5	
13	0.5	
14	0.3	
15	6.8	
16	0.5	
17	0.4	
18	1.4	
19	6.8	
20	4.5	
21	3.4	
22	0.3	

Supplementary Table 5: Horizontal faults heaves for the Iberia southern profile using the SPSI-2. Fault number 1 is the more proximal one.

Double column width

Figure 1
Gómez-Romeu et al

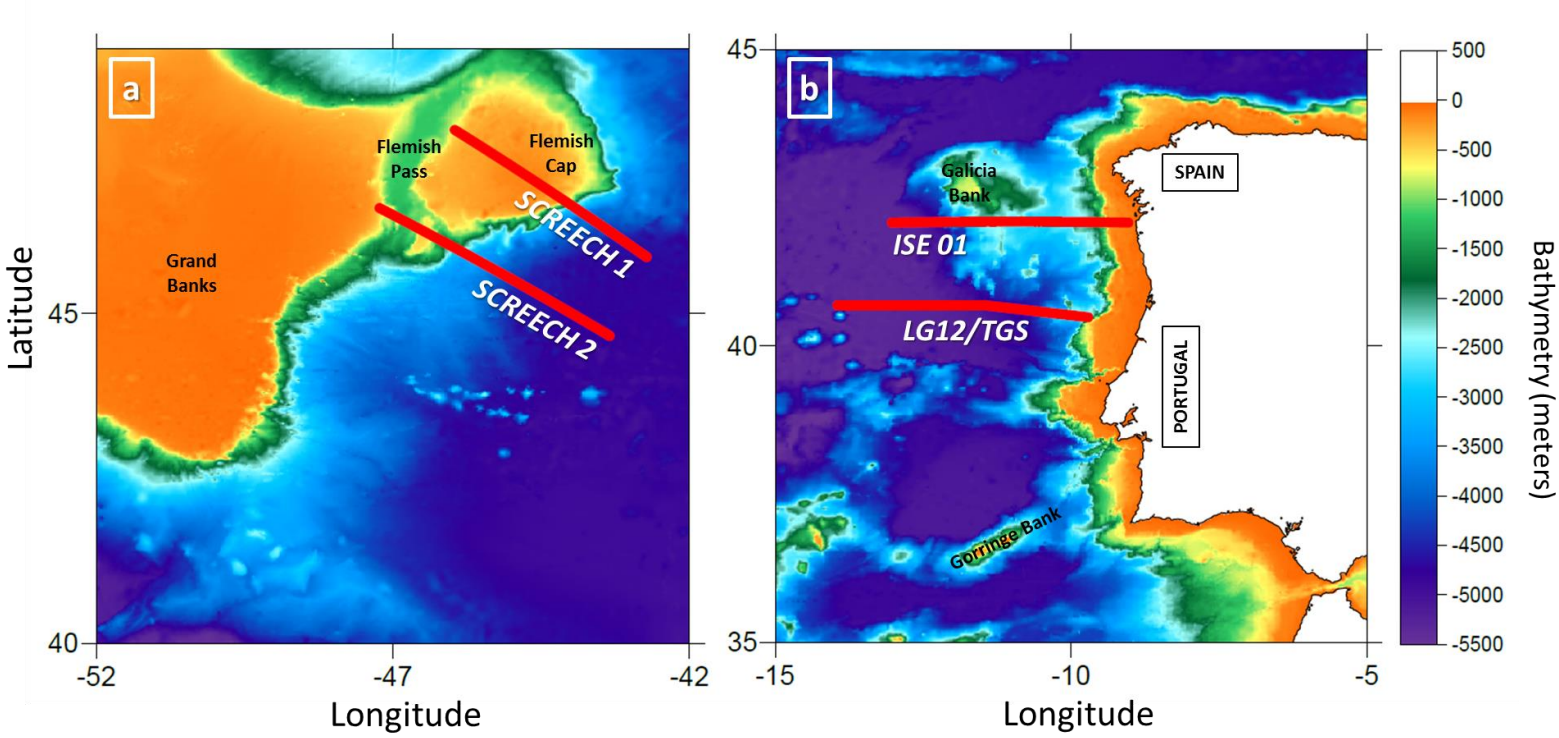

Double column width

Figure 2
Gómez-Romeu et al

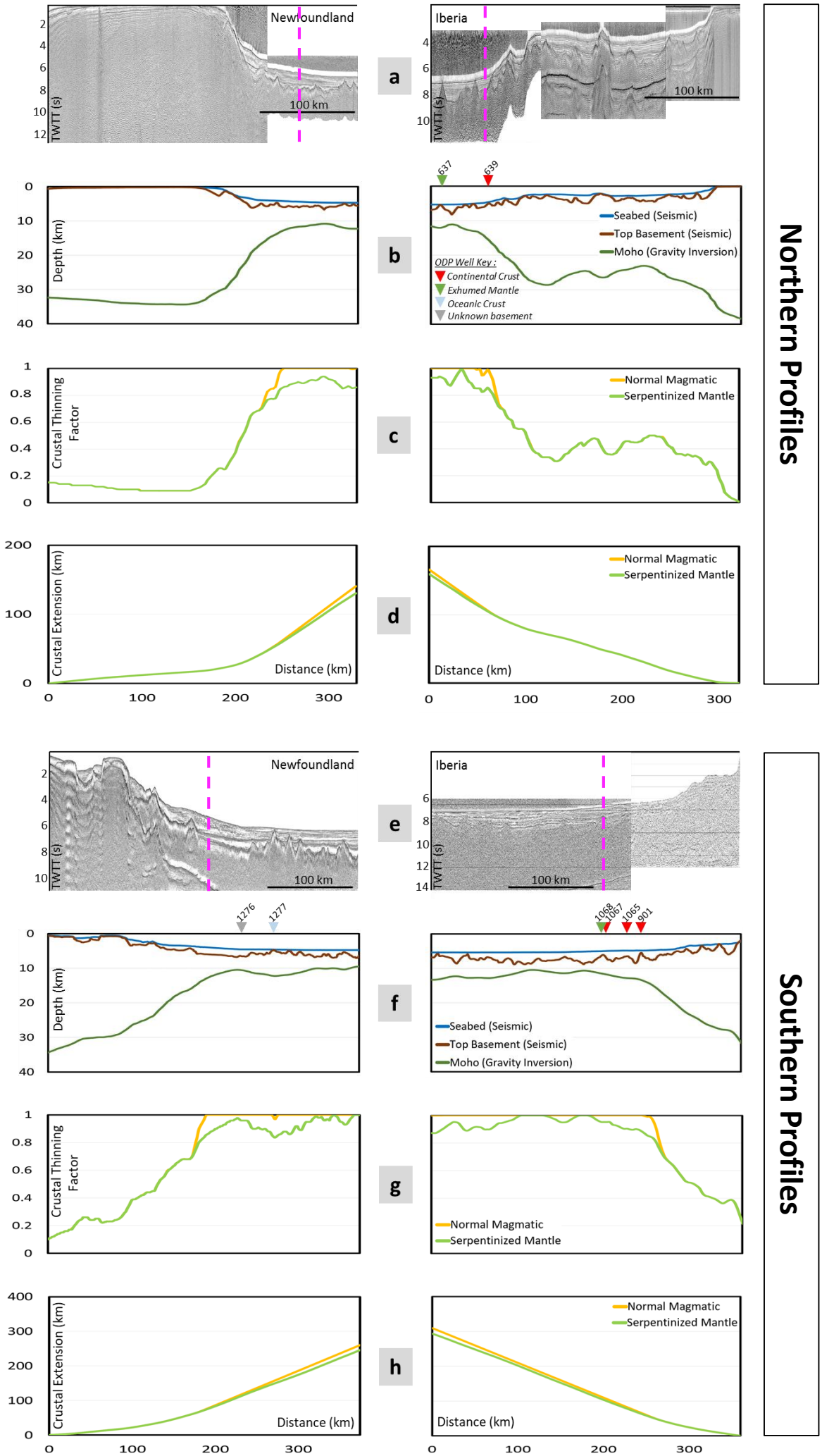

Double column width

Figure 3
Gómez-Romeu et al

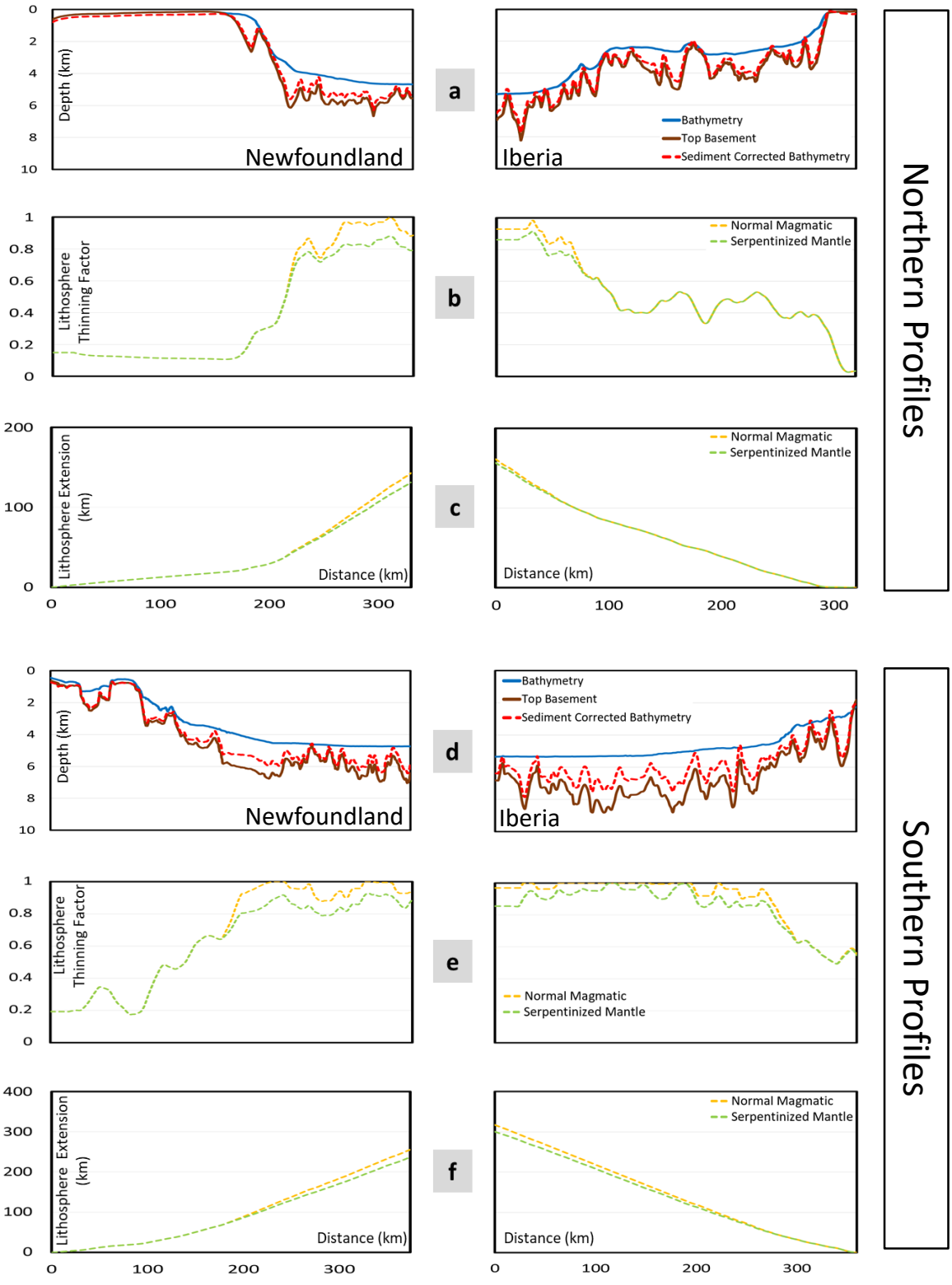

Double column width

Figure 4
Gómez-Romeu et al

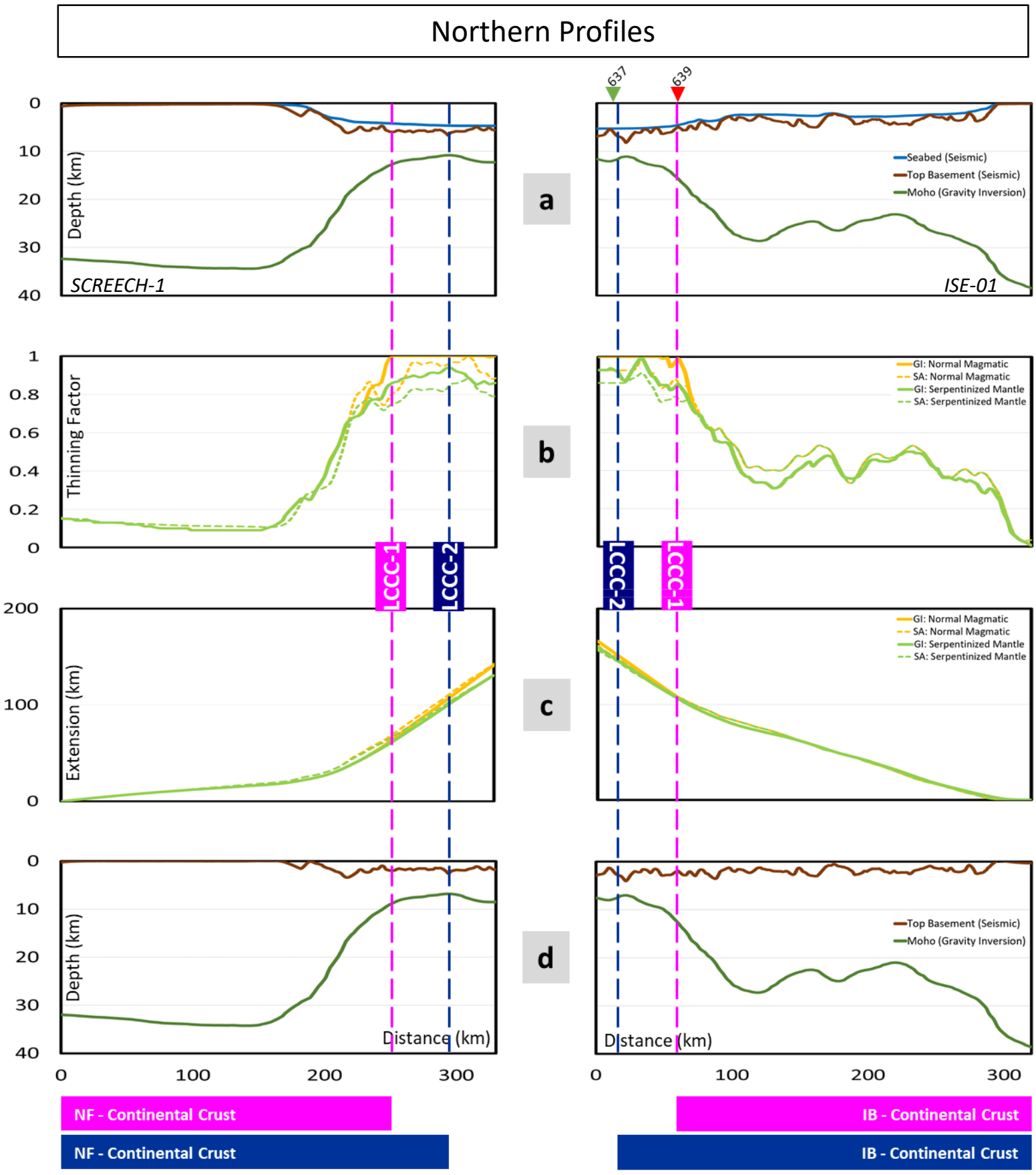

Double column width

Figure 5
Gómez-Romeu et al

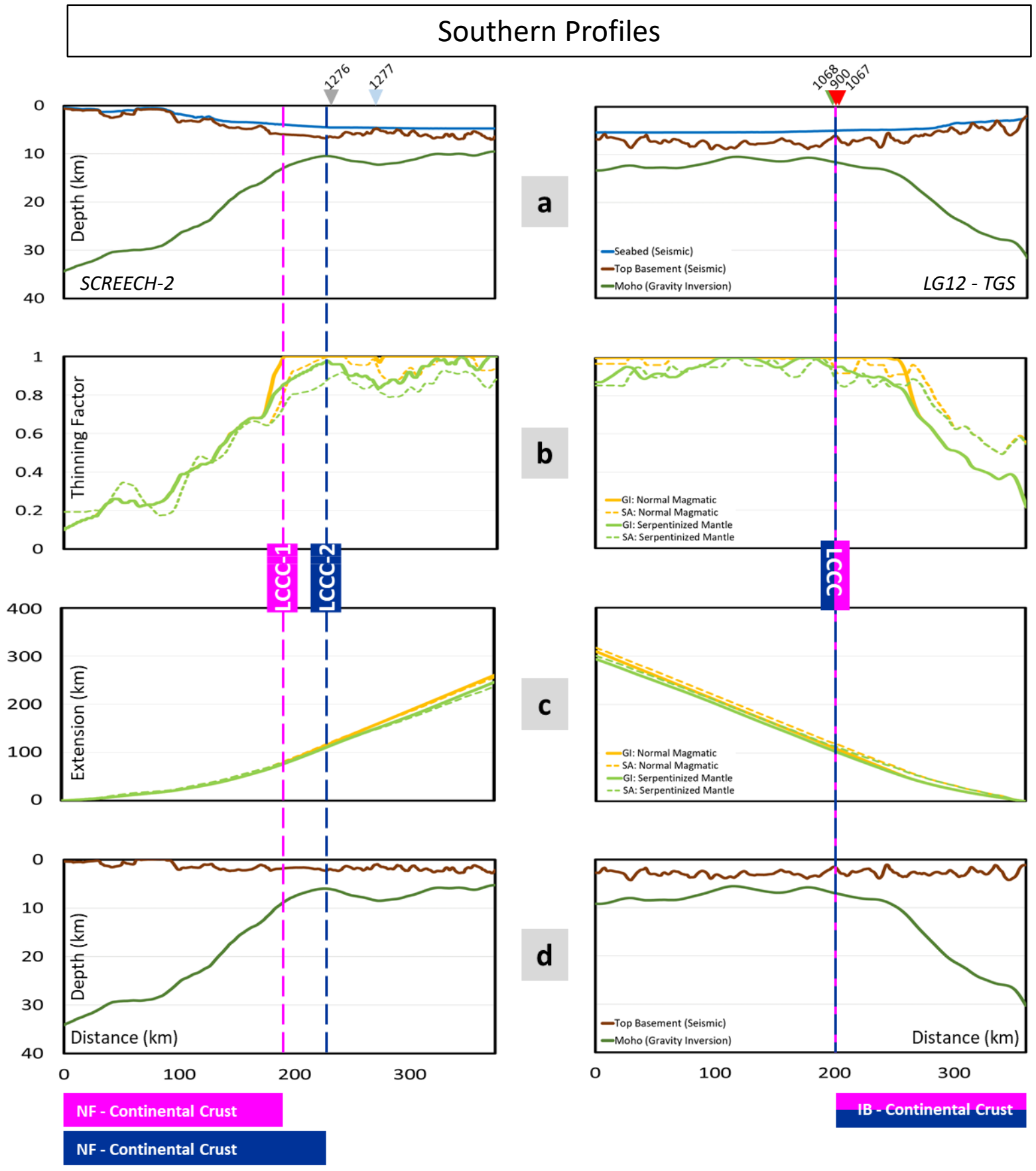

Double column width

Figure 6
Gómez-Romeu et al

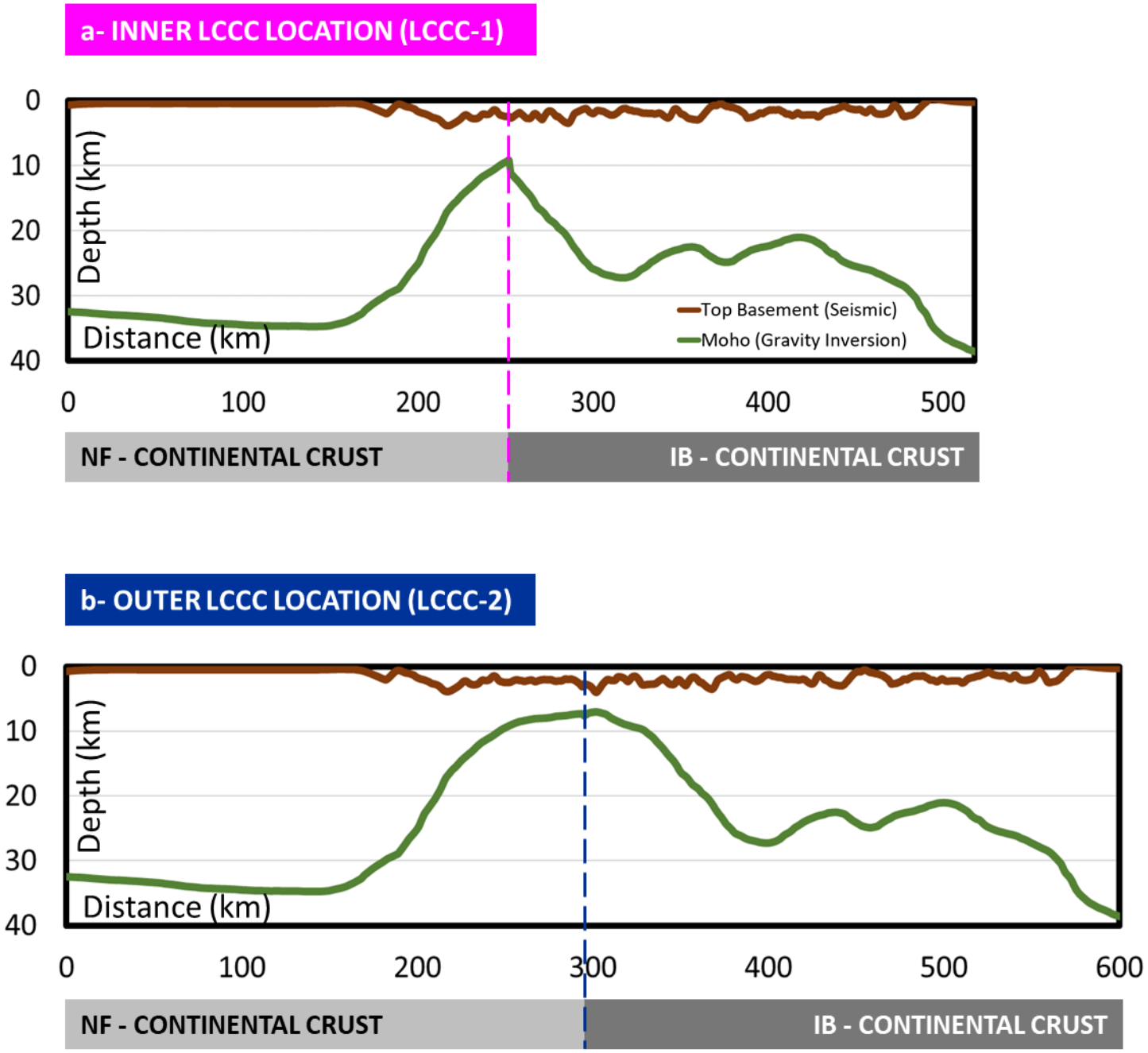

Double column width

Figure 7
Gómez-Romeu et al

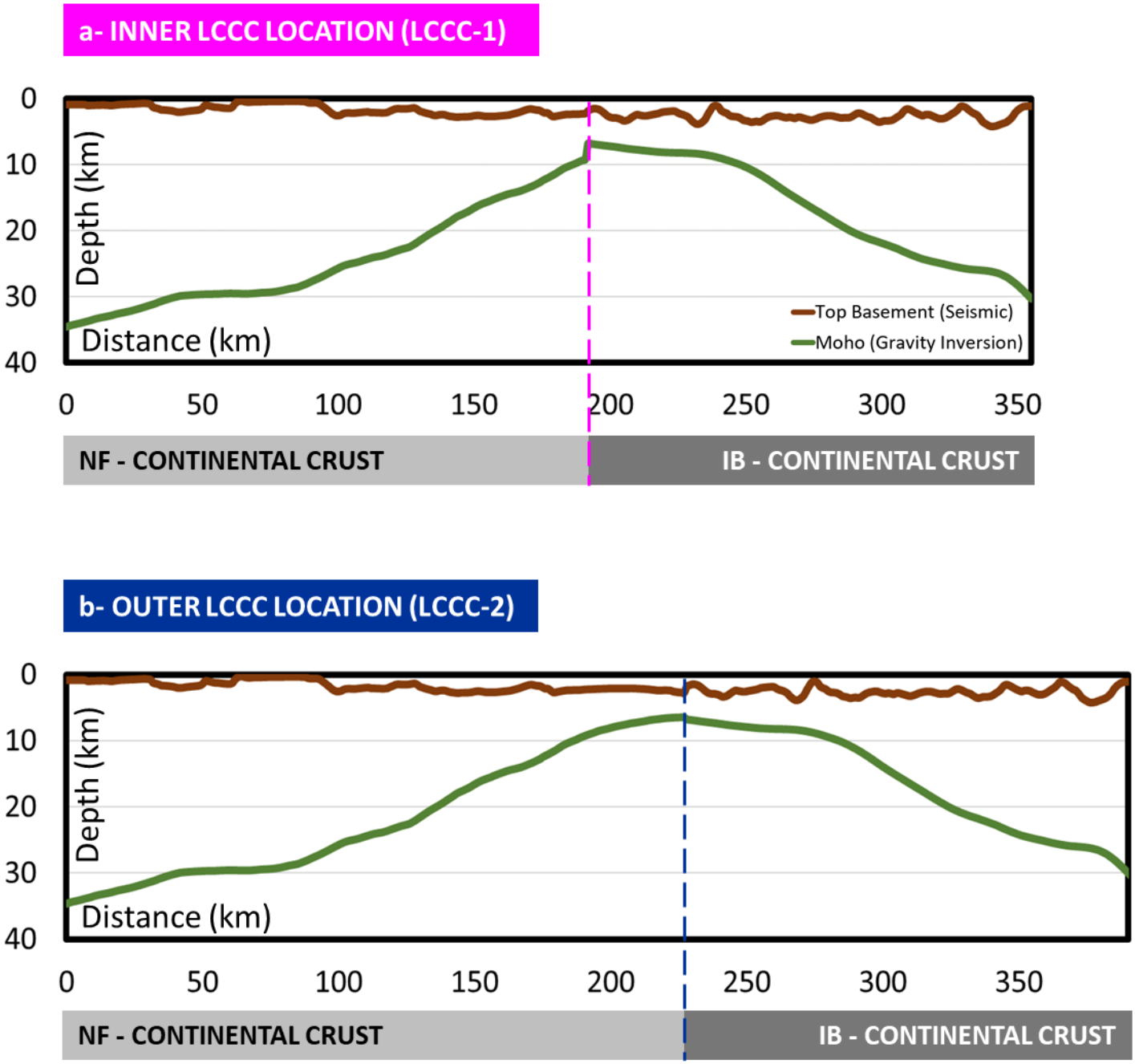

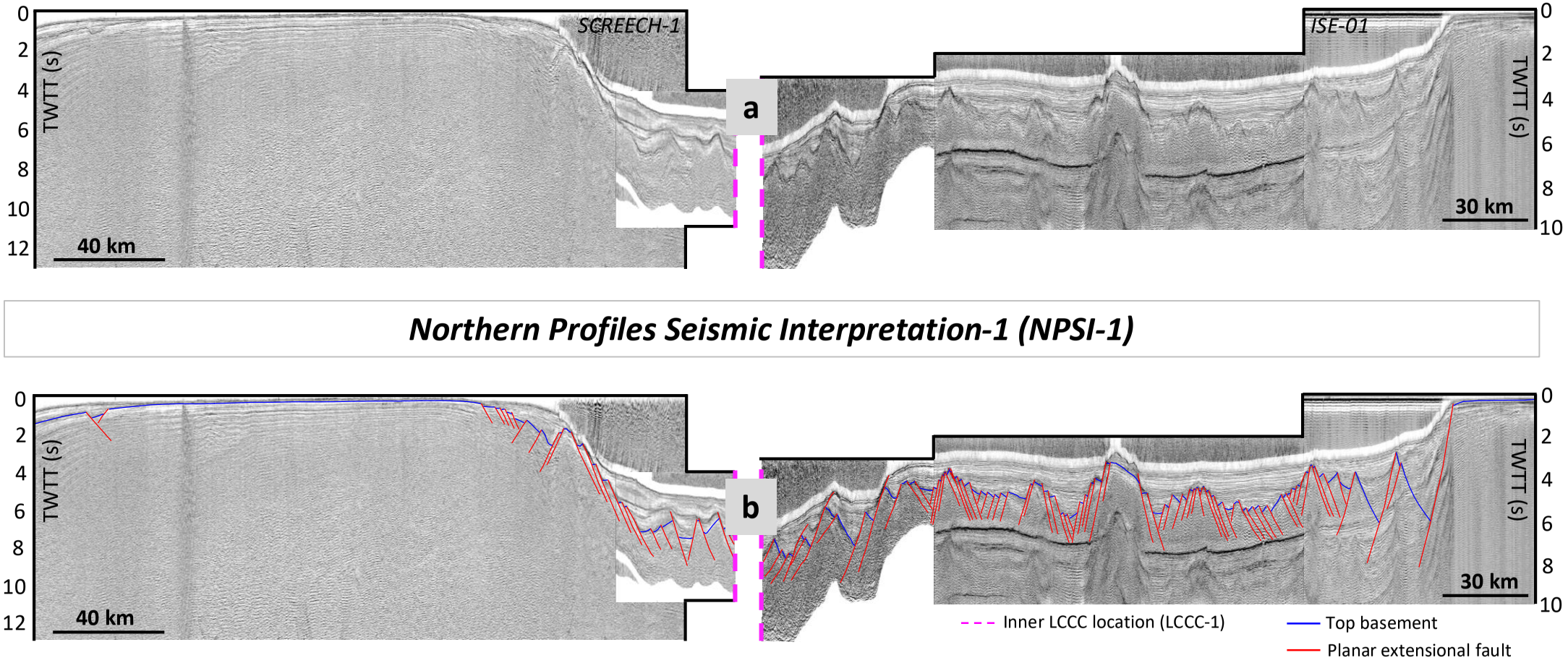

Figure 8
Gómez-Romeu et al

Double column width

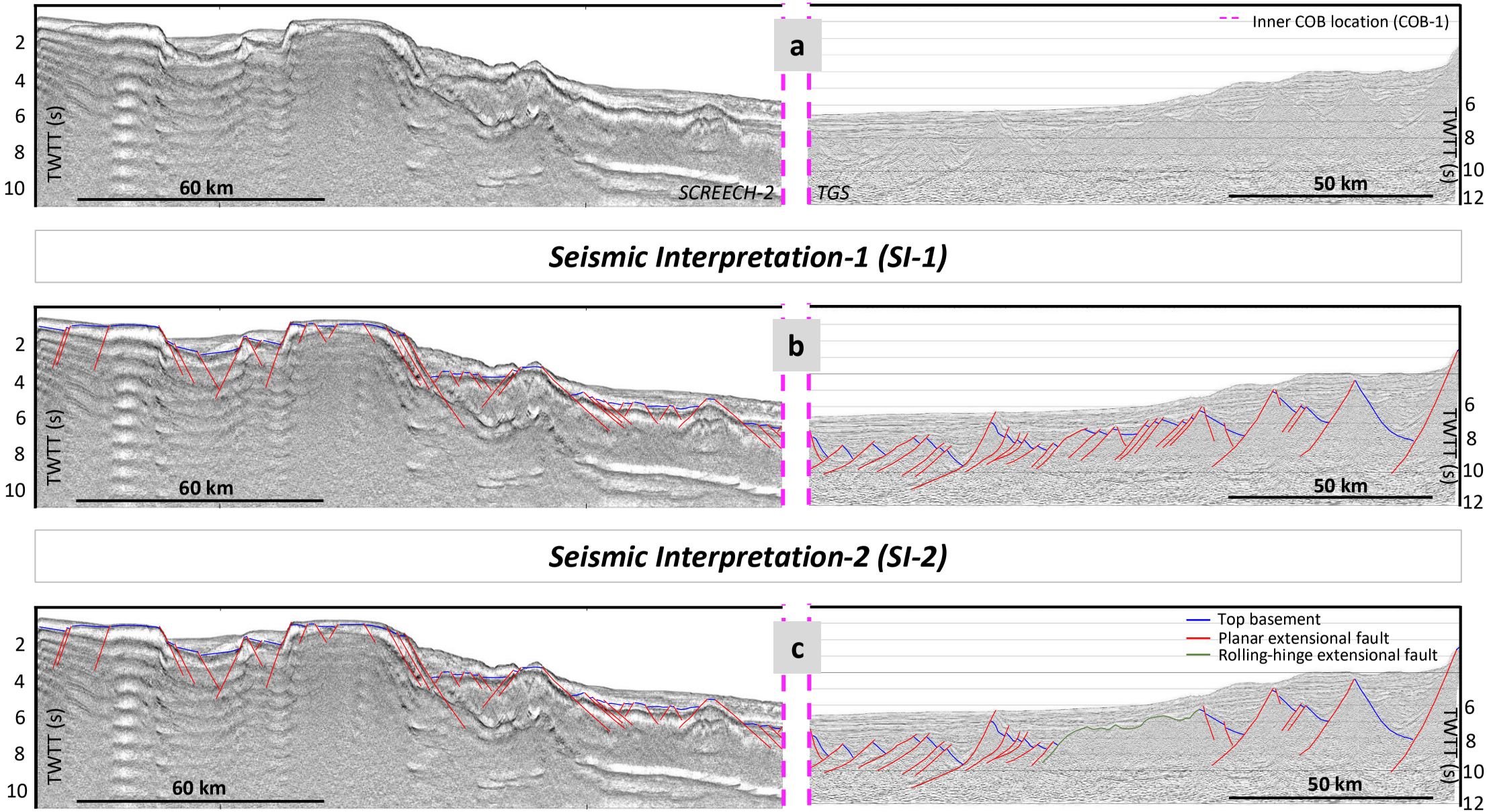

Figure 9
Gómez-Romeu et al

Double column width

Single column width

Figure 10
Gómez-Romeu et al

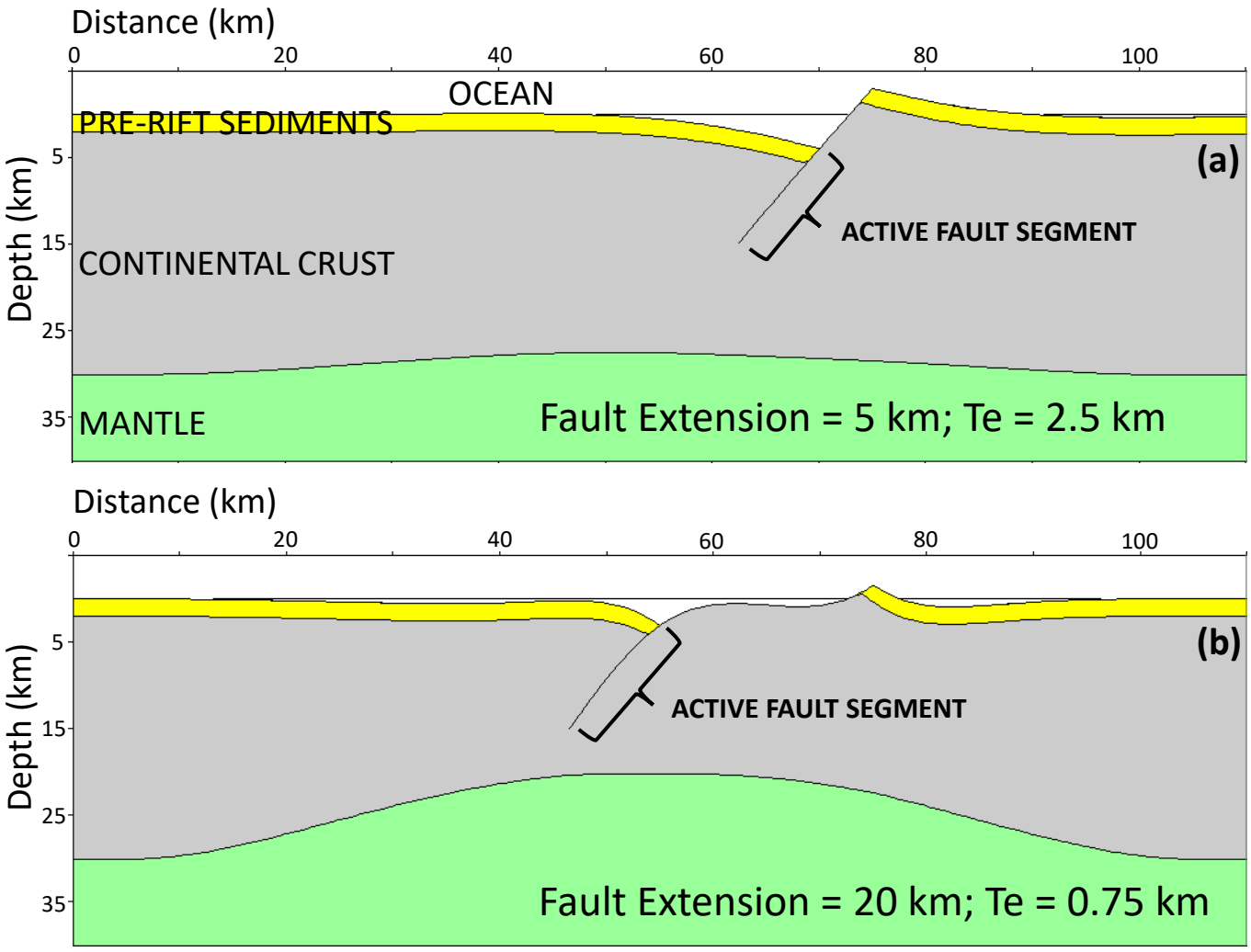

Figure 11

Gómez-Romeu et al

Double column width

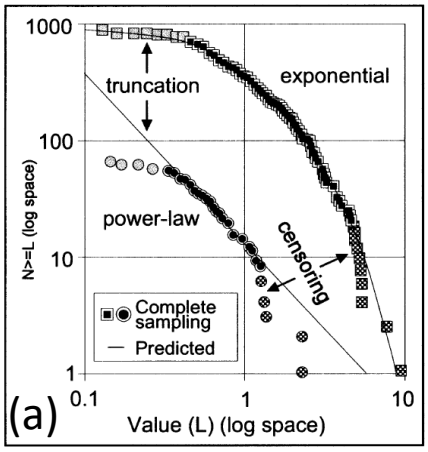

Faults sampled

Power-law relationship

Exponential relationship

Data truncation

Data censoring

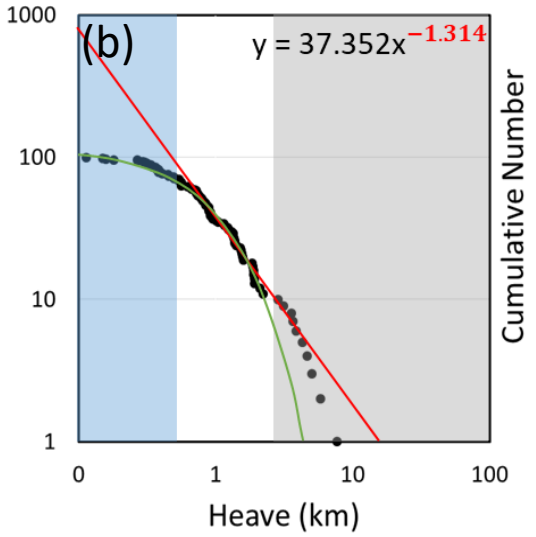

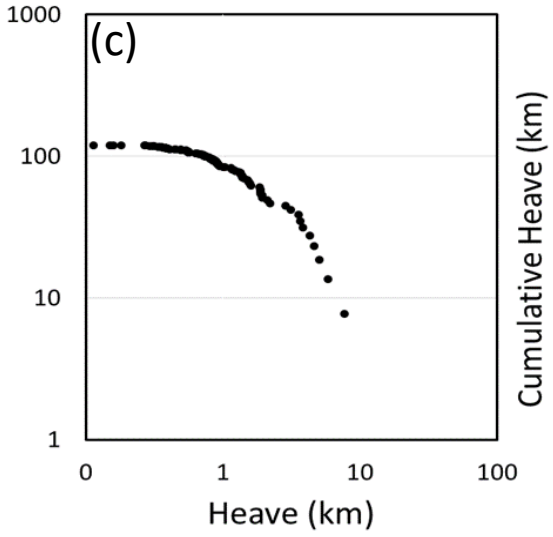

Northern Profiles (NPSI-1)

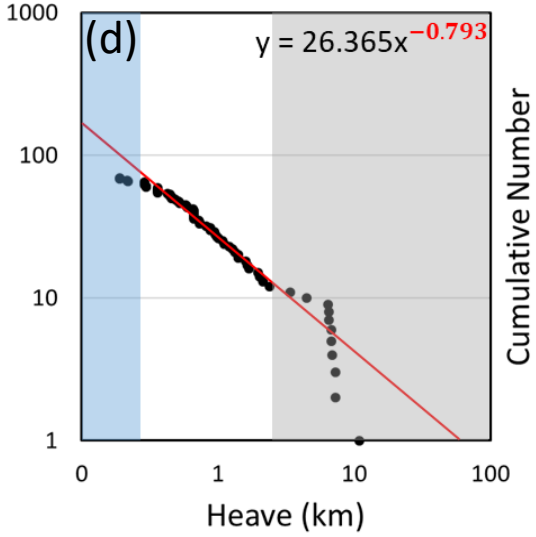

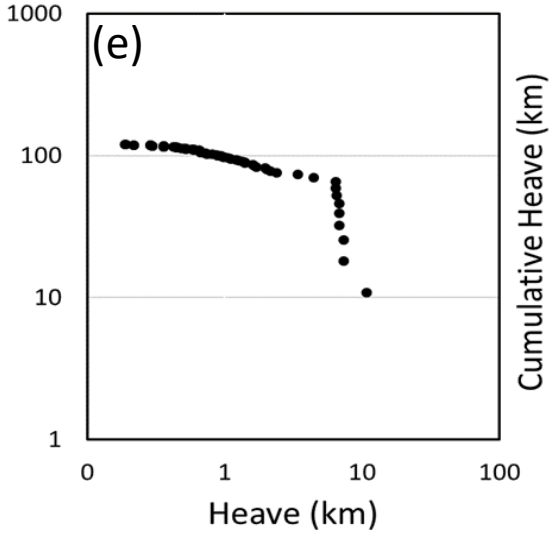

Southern profiles (SPSI-1)

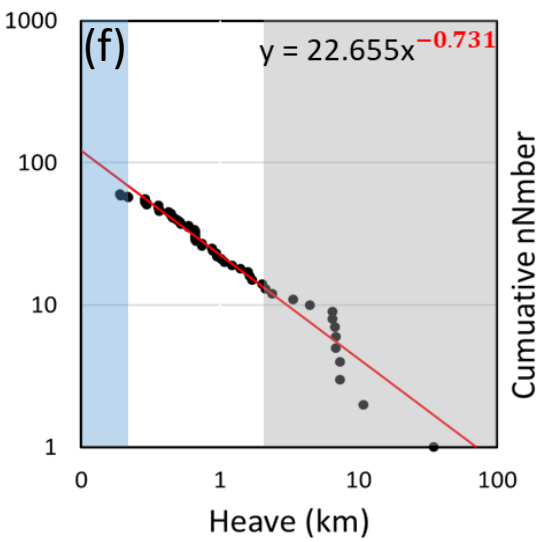

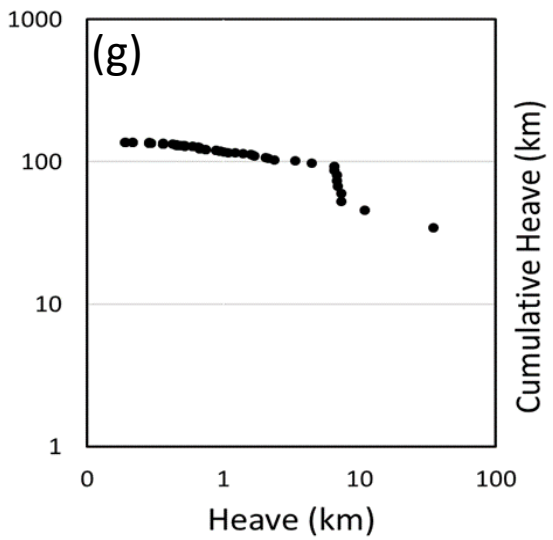

Southern profiles (SPSI-2)

Double column width

Figure 12
Gómez-Romeu et al

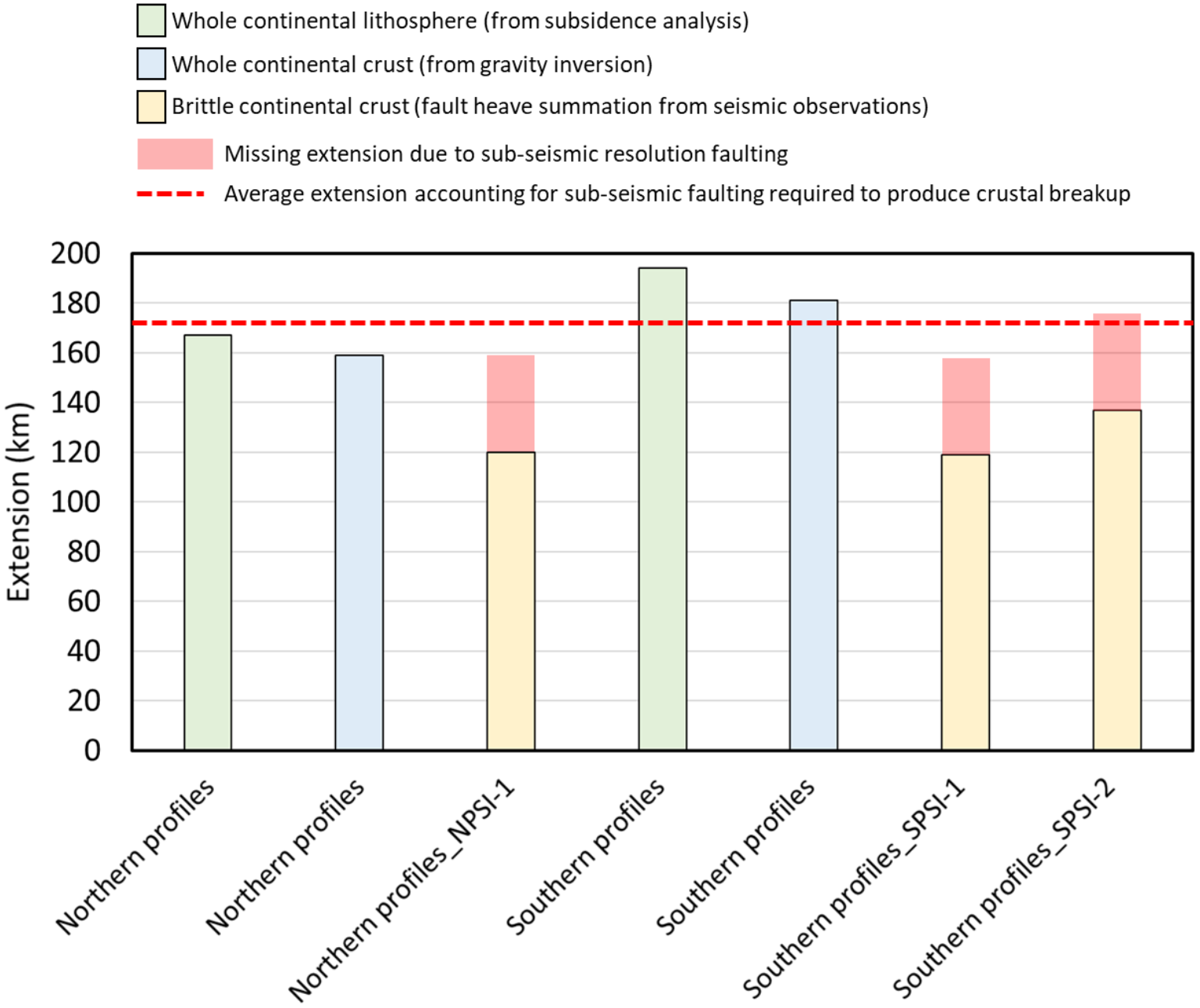

Double column width

Figure 13
Gómez-Romeu et al

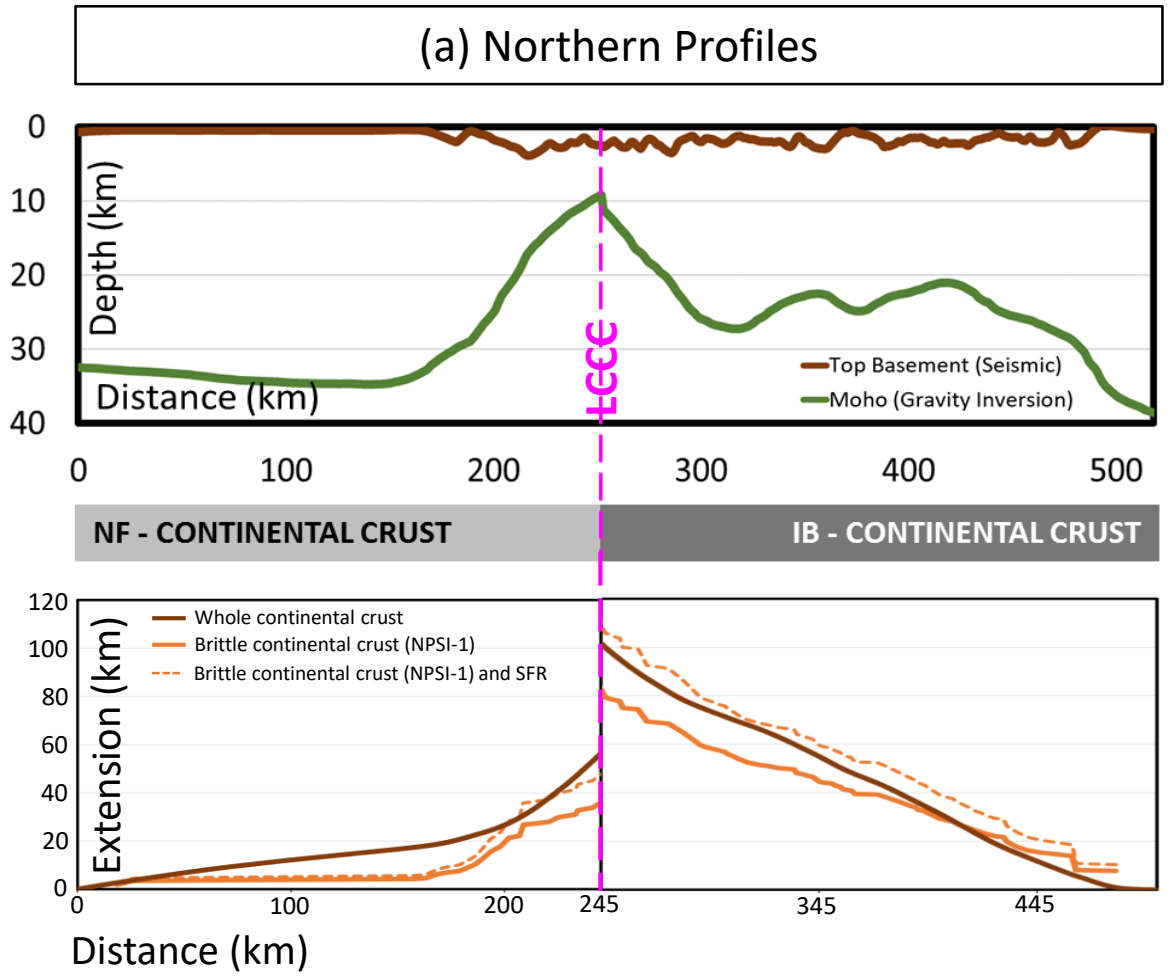

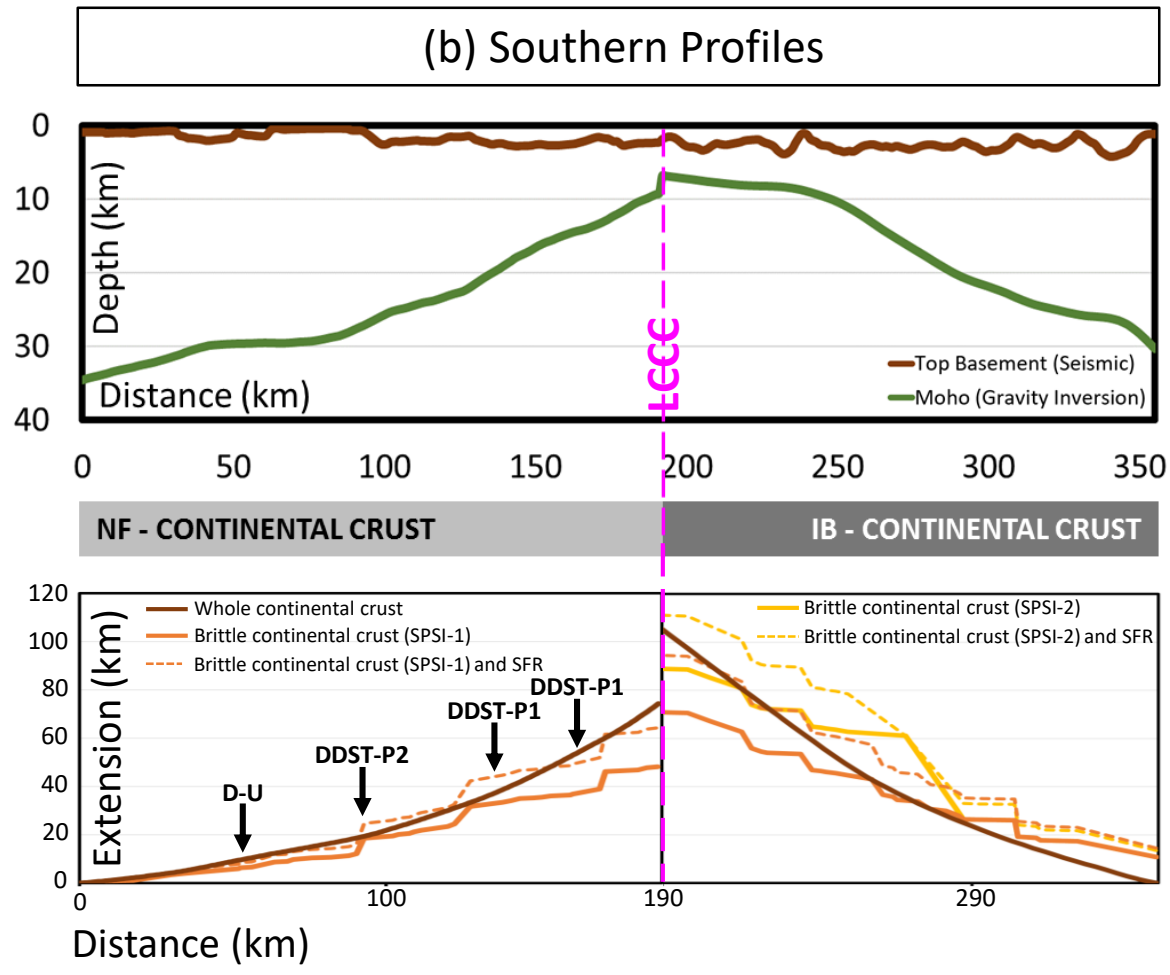

Double column width

Figure 14
Gómez-Romeu et al

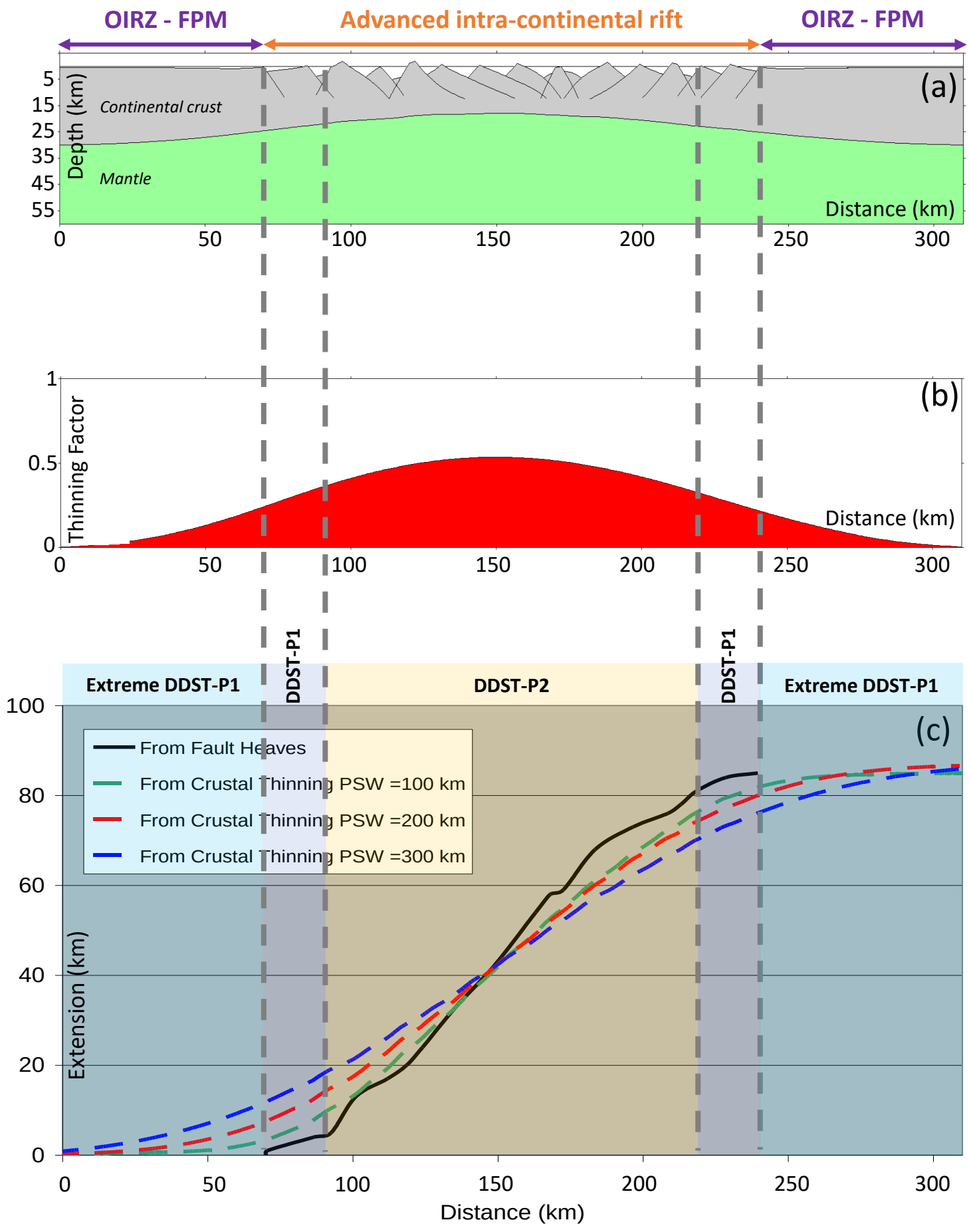

FIGURES CAPTIONS

Figure 1: **a-b)** Bathymetric maps of Iberia and Newfoundland margins. Red lines show the position of SCREECH1 and SCREECH2 seismic profiles on Newfoundland and ISE01 and TGS/LG12 seismic profiles on Iberia.

Figure 2: **a)** and **e)** The northern (SCREECH1 and ISE01, Funck et al., 2003; Zelt et al., 2003) and the southern (SCREECH2 and TGS-LG12, Shillington et al., 2006; Sutra and Manatschal, 2012; Beslier, 1996) seismic profiles. Pink dashed lines show LCCC-1 location. **b)** and **f)** Present-day architecture of the Iberia and Newfoundland margins using sea-bed and top-basement from seismic and Moho depth from gravity anomaly inversion. Numbers and triangles indicate ODP wells (Sawyer et al., 1994; Whitmarsh et al., 1998; Funck et al., 2003). **c)** and **g)** Crustal thinning factor from gravity anomaly inversion. **d)** and **h)** Crustal extension from thinning factor integration.

Figure 3: **a)** and **d)** Bathymetry and top-basement from seismic and sediment corrected bathymetry from flexural backstripping. **b)** and **e)** Lithosphere thinning factor from subsidence analysis. **c)** and **f)** Lithosphere extension from thinning factor integration.

Figure 4: Pink and blue lines show the inner (LCCC-1) and outer (LCCC-2) distal end of contiguous continental crust boundaries respectively. **a)** Present-day architecture of the margin (same as shown in Figure 2b). Numbers and triangles are ODP well data (see Figure 2 for legend). **b)** Thinning factor from gravity anomaly inversion (GI) and subsidence analysis (SA). **c)** Extension from thinning factor integration from gravity anomaly inversion (GI) and subsidence analysis (SA). **d)** Bathymetry and Moho depths for the Iberia and Newfoundland margins restored to the breakup time using a flexural backstripping model.

Figure 5: Pink and blue lines show the inner (LCCC-1) and outer (LCCC-2) distal end of contiguous continental crust boundaries respectively. **a)-d)** Same as in Figure 4 but for the southern profiles.

Figure 6: **a-b)** Bathymetry and Moho depths for the northern Iberia and Newfoundland profiles restored to the breakup time.

Figure 7: **a-b)** Bathymetry and Moho depths for the northern Iberia and Newfoundland profiles restored to the breakup time.

Figure 8: **a)** Northern seismic lines up to the inner-LCCC location (pink line) defined in this study (SCREECH1 and ISE01 seismic profiles, Funck et al., 2003; Zelt et al., 2003). **b)** Seismic interpretation (NPSI-1) of SCREECH1 and ISE01 (top basement and extensional faults are shown).

Figure 9: **a)** Southern seismic lines up to the inner-LCCC location (pink line) defined in this study (SCREECH2 and TGS seismic profiles, Shillington et al., 2006; Sutra and Manatschal, 2012). **b)** Seismic interpretation (SPSI-1) of SCREECH2 and TGS using planar faults (top basement and extensional faults are shown). **c)** Seismic interpretation (SPSI-2) of SCREECH2 and TGS using planar and a rolling-hinge fault (top basement and extensional faults are shown).

Figure 10: Stretch kinematic model showing the lithosphere isostatic response to extensional faulting and crustal thinning. **a)** Planar extensional fault. **b)** Rolling-hinge extensional fault. Fault extension and effective elastic thickness (Te) parameters vary for each fault type.

Figure 11: **a)** Exponential and power-law cumulative frequencies and sampling artifacts distribution from Ackermann et al., (2001). **b-g)** Results of the fault population analysis showing cumulative number versus faults heaves and cumulative heave respect to faults heaves. **b)** A power-law and an exponential frequency curves fitting the sampled faults using the NPSI-1. **d)** and **f)** A power-law frequency curve fitting the sampled faults using the SPSI-1 and SPSI-2 respectively. Equation for the power-law curve is shown for **b)**, **d)** and **f)** (red value corresponds to the fractal dimension).

Figure 12: Summary of the extension estimates required to produce rupture and separation of continental crust along the southern and northern profiles.

Figure 13: **a)-b)** Bathymetry and Moho depths for the Iberia and Newfoundland margins restored to the breakup time (top). Comparison between cumulative extension from proximal to LCCC, from integrated crustal thinning and fault heave summation (bottom). Note that black arrows indicate examples of where D-U, DDST-P1 and DDST-P2 is observed (only the southern Newfoundland profile is used to illustrate these examples but note that they are also observed in the other profiles). **SFR:** Sub-seismic Fault Resolution; **D-U:** Depth-uniform stretching and thinning; **DDST-P1:** Depth-Dependent Stretching and Thinning Polarity 1; **DDST-P2:** Depth-Dependent Stretching and Thinning Polarity 2.

Figure 14: Illustration of Depth-Dependent Stretching and Thinning. **a)** Stretch kinematic model showing an advanced stage of intra-continental rift with a pure-shear width of 200 km associated to each fault. **b)** The thinning factor profile across the profile shown in a). **c)** Cumulative extension of the section shown in a) from fault heaves and total integrated crustal thinning using a pure-shear width of 100, 200 and 300 km respectively. **OIRZ – FPM:** Outboard Intra-continental Rift Zone – Future Proximal Margin; **PSW:** Pure-shear width; **Extreme DDST-P1**: Extreme Depth-Dependent Stretching and Thinning Polarity-1; **DDST-P1**: Depth-Dependent Stretching and Thinning Polarity-1; **DDST-P2:** Depth-Dependent Stretching and Thinning Polarity-2.